skb.se

SKB TR-26-06

ISSN 1404-0344
ID 2091277
June 2026

Äspö Hard Rock Laboratory
Concrete and Clay
Long-term corrosion studies
Final report

Per Mårtensson, Svensk Kärnbränslehantering AB
Mariusz Kalinowski, RISE – Research Institutes of Sweden AB

Keywords: Concrete, Corrosion, Metal, Aluminium, Zinc, Iron, Steel

A pdf version of this document can be downloaded from www.skb.se

Summary

This report constitutes the final report of the long-term studies of metal corrosion carried out within the project *Concrete and Clay* during the years 2010 to 2025 in the Äspö Laboratory's underground facility.

The report summarises the results from studies of corrosion of aluminium, zinc, carbon-steel and stainless-steel objects which have been embedded in concrete and stored under repository-like conditions, i.e. cementitious and reducing conditions, for up to 15 years.

In summary, the experiments have shown that:

- Zinc reacts vigorously with the fresh concrete during casting of the concrete cylinders, and a porous zone is formed adjacent to the metal surface. As the corrosion process proceeds, the pores in this zone is filled with corrosion products and a dense layer consisting of, among others, $Ca(OH)_2$ and $Zn(OH)_2$ is formed. This layer reduces the zinc corrosion rate significantly and the corrosion process in principle comes to a halt once this solid layer has formed.

  Even though the experiments have not been designed to accurately determine the corrosion rate for zinc, it is assessed that the average corrosion rate for zinc over the 15-year duration of these experiments is significantly lower than that of one millimetre per year assumed in the latest valid safety assessment when this project was initiated and which motivated this study.

- Like zinc, aluminium reacts vigorously with the fresh concrete during casting of the concrete cylinders, and a porous zone is formed adjacent to the metal surface. As the corrosion process proceeds, the pores in this zone is filled with corrosion products and a dense layer consisting of, among others, $Ca(OH)_2$ and $Al(OH)_3$ is formed. This layer reduces the aluminium corrosion rate significantly and the corrosion process in principle comes to a halt once this solid layer has formed.

  Thanks to this layer of reaction products, the average corrosion rate for aluminium over the 15-year duration of these experiments has been significantly lower than that of one millimetre per year assumed in the latest valid safety assessment when this project was initiated and which motivated this study.

- Corrosion of carbon steel is very slow, and no signs of corrosion have been identified in this study.

- Corrosion of stainless steel is very slow, and no signs of corrosion have been identified in this study.

Sammanfattning

Denna rapport utgör slutrapporten från de långtidsstudier av metallkorrosion som genomförts inom projekt *Concrete and Clay* under åren 2010 till 2025 i Äspölaboratoriets underjordsanläggning.

Rapporten sammanfattar resultaten från studier av korrosion av prover av aluminium, zink, kolstål och rostfritt stål som har ingjutits i betong och lagrats under förvarsliknande förhållanden, alltså cementbaserade och reducerande, i upp till 15 år.

Studierna har visat följande:

- Zink reagerar kraftigt med den färska betongen vid gjutning av betongcylindrarna och en porös zon bildas i angränsning till metallytan. Denna zon fylls efterhand av reaktionsprodukter från korrosionsprocessen och ett tätt lager bestående av bland annat $Ca(OH)_2$ och $Zn(OH)_2$ bildas vilket medför att korrosionsprocessen mer eller mindre avstannar.

  Även om genomförda experiment inte varit utformade för att noga bestämma korrosionshastigheten hos de olika metallerna så är bedömningen den att den genomsnittliga korrosionshastigheten för zink under de 15 år som dessa experiment pågått varit signifikant lägre än den antagna hastigheten på en millimeter per år som antogs i den säkerhetsanalys som nyligen genomförts när detta projekt initierades och vilken motiverade denna studie.

- Liksom zink reagerar aluminium kraftigt med den färska betongen vid gjutning av betongcylindrarna och en porös zon bildas i angränsning till metallytan. Denna zon fylls efterhand med reaktionsprodukter från korrosionsprocessen och ett tätt lager bestående av bland annat $Ca(OH)_2$ och $Al(OH)_3$ bildas vilket medför att korrosionsprocessen mer eller mindre avstannar.

  Liksom för zink är bedömningen den att korrosionshastigheten för aluminium under de 15 år som dessa experiment pågått varit betydligt lägre än den på en millimeter per år som antogs i den säkerhetsanalys som nyligen genomförts när detta projekt initierades och vilken motiverade denna studie.

- Korrosion av kolstål är mycket långsam och inga tecken på korrosion har kunnat identifieras i denna studie.

- Korrosion av rostfritt stål är mycket långsam och inga tecken på korrosion har kunnat identifieras i denna studie.

Contents

1 Introduction

1.1 Background

Low- and intermediate-level radioactive waste is disposed in the final repository for short-lived radioactive waste, SFR, or stored temporarily while waiting for the final repository for long-lived radioactive waste to be constructed. The waste consists of a mixture of different types of materials including both organic as well as inorganic materials with metals and ion-exchange resins making up a significant portion of the total amount of waste.

Prior to disposal, the waste is placed in one of several types of containers which in addition to the waste also may contain conditioning materials such as cement, cementitious grout or bitumen. However, ion exchange resins disposed in the waste vaults for concrete tanks, 1BTF and 2BTF are only dewatered without any conditioning materials.

In SFR, which was taken into operation 1988 (the silo in 1991), concrete and other cement-based materials are extensively used in the engineered barrier system, either alone or in combination with bentonite as in the silo (SKB 2023a).

For the long-lived low- and intermediate-level radioactive waste, SKB (2019) analysed the performance of a barrier system comprising concrete barriers and a combination of a concrete structure and bentonite for the PWR reactor internals and the legacy waste currently stored at the Studsvik site respectively.

Post-closure, the waste will chemically interact with the materials in the engineered barriers, the groundwater as well as species dissolved in the groundwater. Through these processes, both radionuclides and chemical species from the degrading waste will be released into the groundwater and available for transport out of the repository. In addition, also other reaction products formed in these processes may form.

In the safety analyses undertaken at facilities planning, construction, operation and before their final closure, detailed knowledge of the abovementioned processes is required. To increase SKB's knowledge and understanding of some of these processes, the project *Concrete and Clay* has been carried out during the years 2010–2025.

1.2 Metal corrosion

Reinforcement bars, tie rods and other steel objects embedded in the engineered barriers as well as metals present in the waste such as zinc and aluminium but also iron and steel, will corrode during both the operational period and post-closure.

The impact of metal corrosion depends on type of metal, type of corrosion process (aerobic or anaerobic), corrosion rate and whether soluble or insoluble corrosion products are formed. The molar volume of insoluble corrosion products is often significantly larger than that of the metal/alloy (SKB 2023b, Figure 3-7).

The often most visible effects of metal corrosion are discoloration of the concrete surface and concrete spalling caused by the formation of voluminous corrosion products on the metal objects embedded in the concrete structure, as shown in Figure 1-1. For corrosion of the reinforcement bars within a concrete structure, this leads to a loss of function of the reinforcement bars and a reduced load-bearing capacity of the concrete structure. See (Höglund 2014 and SKB 2023c) for more details.

If the corrosion products instead dissolve in the concrete porewater, voids may form between the metal and the concrete with the formation of a permeable zone and reduced load-bearing capacity of the structure as consequences.

Figure 1-1. *Concrete spalling due to corrosion of reinforcement bars.*

The impact of metal corrosion is not restricted to the direct effects discussed above. Through anaerobic metal corrosion, hydrogen gas is formed through the reaction exemplified by the anaerobic corrosion of iron, Equation 1-1:

$$3\ Fe(s) + 4\ H_2O \rightarrow Fe_3O_4(s) + 4\ H_2(g) \qquad \text{Eq. 1-1}$$

The consequences of this reaction are dependent on the reaction rate and hence the rate of gas formation.

In SKB (2008), the valid safety assessment at the time project *Concrete and clay* was planned and the experiments installed, a corrosion rate of one millimetre per year was assumed for aluminium and zinc. The consequence of such a high corrosion rate is that large amounts of hydrogen gas would form soon after closure. If this gas cannot be effectively transported out of the waste domain, a high gas pressure will form inside the concrete structures with an increased risk for cracking and potential fast gas-driven advection and release of radionuclides as consequences. To ensure controlled gas release, gas evacuation systems are planned to be installed in the lids of the concrete structures in 2BMA and the silo and currently also considered for 1BMA.

For iron and steel, the long-term corrosion rate under anoxic alkaline conditions is expected to be 0.001–0.1 µm/year (SKB 2023d, Chapter 5) and hence the rate of gas formation is considerably lower than assumed for corrosion of aluminium and zinc. Therefore, the requirements on the gas transport capacity of the gas evacuation systems are lower when considering only corrosion of iron and steel.

1.3 Project *Concrete and Clay* – project objectives

The objective of project *Concrete and clay* was to increase SKB's understanding of the processes that occur when the waste, conditioning grout and the engineered-barriers materials interact under the influence of an anoxic groundwater. During planning of this project, the following processes were considered:

- Metal corrosion, with focus on studying the evolution of the corrosion process for aluminium and zinc but also carbon steel and stainless steel were studied.
- Diffusion of metal ions in a cement-based matrix.
- Degradation of certain organic materials representative for low- and intermediate level radioactive waste such as ion exchange resins and filter aid materials, protective clothing (gloves, cotton) or paper in a cement-based matrix.

- Transport of organic degradation products in a cement-based matrix,
- Diffusion of metal ions in bentonite.
- Mineral alterations at the concrete/bentonite interface.

This report presents the results from long-term corrosion studies which includes the first two bullet points in the list above whereas the other parts of the project are (or will be) reported separately. See e.g. Szabó et al. (2020) and Mårtensson and Kalinowski (2019).

1.4 Long-term corrosion studies - Experimental concept

The long-term corrosion studies were designed to simulate the conditions in a repository for radioactive waste comprising a concrete barrier system after closure. The metal objects were therefore embedded in concrete without prior cleaning or removal of and existing corrosion products. For all metals, triplicates were installed to facilitate studies of the evolution of the corrosion process, especially important for zinc and aluminium.

Three concrete cylinders – each containing metal objects of both zinc, aluminium, carbon steel or stainless steel - were installed in holes in the tunnel floor in two locations in the underground facility of the Äspö Hard Rock Laboratory i.e. TASR and NASA2861A during 2010 and 2011 (Chapter 2).

Two of the concrete cylinders were installed in holes with access to groundwater whereas the third concrete cylinder was installed in a nominally dry hole, i.e. a hole which had been found not to be intersected by water-bearing fractures, Table 3-3.

The concrete cylinders were retrieved and analysed at five, ten and fifteen years after installation, respectively, Chapter 4.

1.5 This report

1.5.1 Purpose of this report

This report constitutes the final report for the long-term corrosion studies performed within the framework of the project *Concrete and Clay*. The purpose of this report is to present a detailed summary of the work covering all aspects from casting of the concrete cylinders containing the metal objects, installation, retrieval and analysis and finally to present the project conclusions.

The following topics are covered in this report:

- Preparation and characterisation of the tunnel niches for the experiments.
- Materials used in the experiments.
- Casting of the concrete cylinders.
- Installation of the concrete cylinders in the holes in the tunnel floor.
- Retrieval and sectioning of the concrete cylinders.
- Material analyses.

1.5.2 Structure

This report comprises in total ten chapters and one appendix with the following content

Chapter 1 gives a background and motivation for the project *Concrete and Clay.*

Chapter 2 presents the experimental sites.

Chapter 3 presents materials and methods used for casting and installation of the concrete cylinders.

Chapter 4 presents the methods used for retrieval and sectioning of the concrete cylinders.

Chapter 5 presents the methods used for preparation of specimens for analysis as well as methods and instruments used.

Chapter 6 presents the results from long-term corrosion studies of zinc.

Chapter 7 presents the results from long-term corrosion studies of aluminium.

Chapter 8 presents the results from long-term corrosion studies of carbon steel.

Chapter 9 presents the results from long-term corrosion studies of stainless steel.

Chapter 10 summaries the work presented in this report and presents project conclusions.

Appendix 1 presents a compilation of the results from the analyses of the chemical composition of cement paste at various distances from the metal objects.

2 Experimental sites

Two different sites were used for the long-term corrosion experiments conducted within the project *Concrete and Clay*: TASR and NASA2861A.

2.1 TASR

2.1.1 Location and overview

TASR is located 507 meters down in the main tunnel of the Äspö Hard Rock Laboratory at a depth of – 69 meters, Figure 2-1 and connects directly to NASA0507. TASR is about 10 meters deep and about 5 meters in height. An illustration is shown in Figure 2-2. Due to a misunderstanding during installation of the experiments, Mårtensson (2015) reports that the concrete cylinders were installed in holes in NASA0507. This has been corrected and in this report the location of these experiments is correctly reported as TASR.

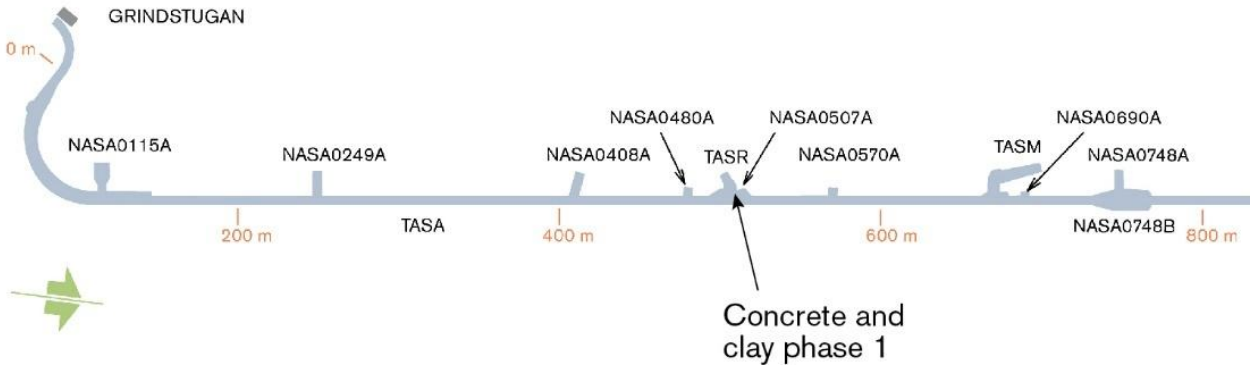

***Figure 2-1**. Location of NASA0507A and TASR.*

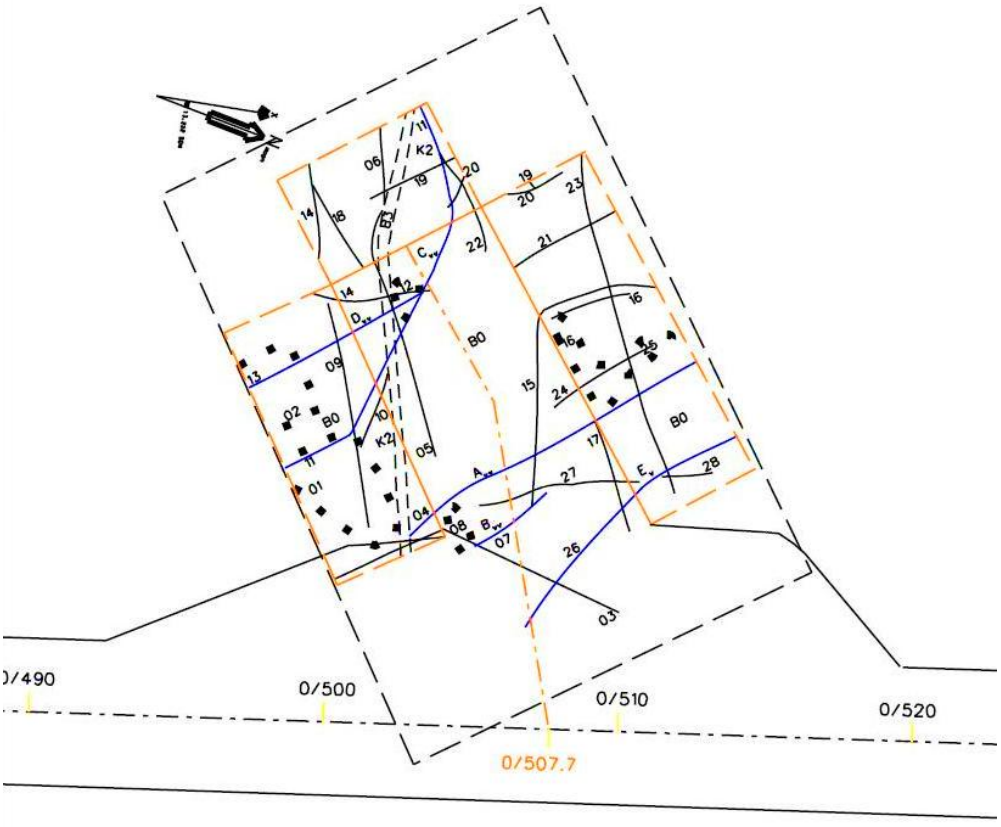

***Figure 2-2.** A schematic illustration of NASA0507A and TASR showing both the tunnel floor and walls. Blue lines illustrate water-bearing fractures whereas black lines illustrate dry fractures.*

2.1.2 Site characterisation

When TASR was made available to the project it had previously been mapped and found to contain a few water-bearing fractures with water flows between 0.003 and 0.04 l/min each. Based on these results, two pilot holes (KR0009G01 and KR0013G01) each with a diameter of 76 mm were drilled into the tunnel floor. During this work it was noticed that KR0013G01 intersected with a fracture that reached the tunnel floor. As this introduced a risk that oxygen-containing groundwater could penetrate the installation hole and affect the experiment, KR0013G01 was abandoned and a new hole, (KR0014G01) was drilled. The depth of KR0009G01 and KR0014G01 was 4.4 and 4.8 meters respectively.

The cores were photographed both dry and wet and a core mapping protocol was prepared. A photograph of the wet cores from KR0009G01 also representative for KR0014G01 is shown in Figure 2-3.

Figure 2-3. *A photograph of the cores from KR0009G01.*

After measuring the groundwater pressure in the pilot holes, Table 2-1, the pilot holes were over-cored to ∅ 350 mm and a depth of about 3.7 and 3.9 meters for KR0009G01 and KR0014G01 respectively.

Table 2-1. Groundwater pressure in the pilot bore holes in NASA0507A/TASR.

Pilot bore hole	Groundwater pressure (bar)
KR0009G01	2
KR0014G01	2.5

The composition of the groundwater in the bedrock surrounding TASR is significantly influenced by intruding meteoric surface water. Table 2-2 presents average values for selected groundwater components from analyses carried out during the years 2010 to 2020.

Table 2-2. Groundwater composition in TASR.

Component	Concentration (mg/l)
Cl^-	758.4
SO_4^{2-}	75.8
Na^+	434.3
Ca^{2+}	157.2
DOC	13.7
pH	7.5

2.2 NASA2861A

2.2.1 Location and overview

NASA2861A is located 2861 meters down in the main tunnel at a depth of −383 meters, Figure 2-4. An illustration of the niche is shown in Figure 2-5.

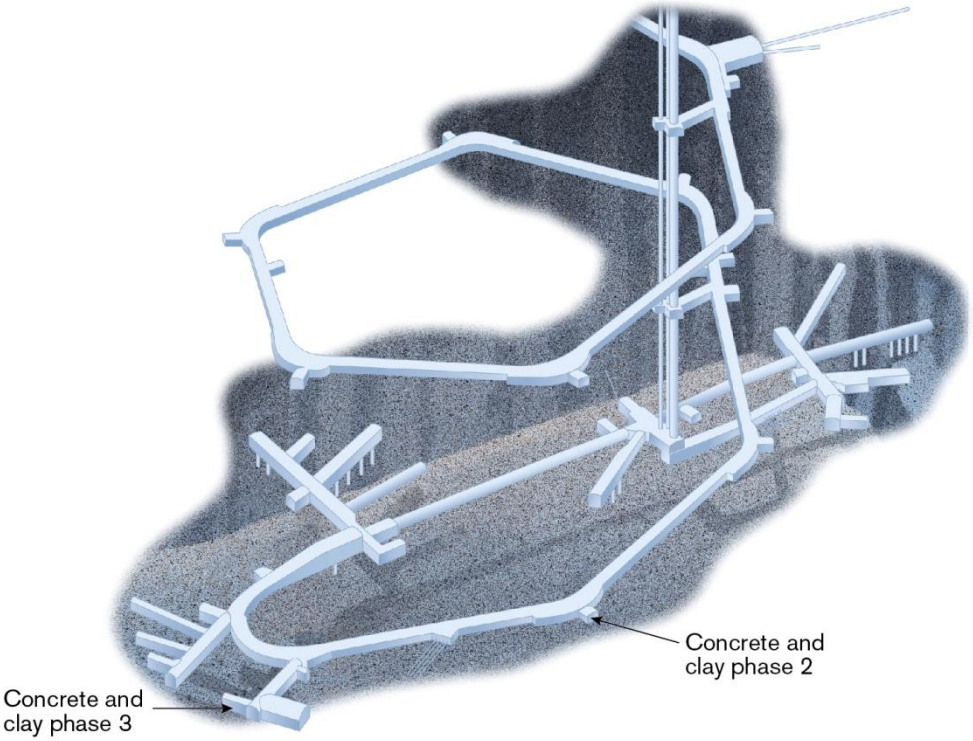

***Figure 2-4**. Location of NASA2861 (labelled Concrete and clay phase 2). Also shown is the location of the field scale bentonite experiments (labelled Concrete and clay phase 3) conducted within this project but not included in this report. See Mårtensson (2015) for details.*

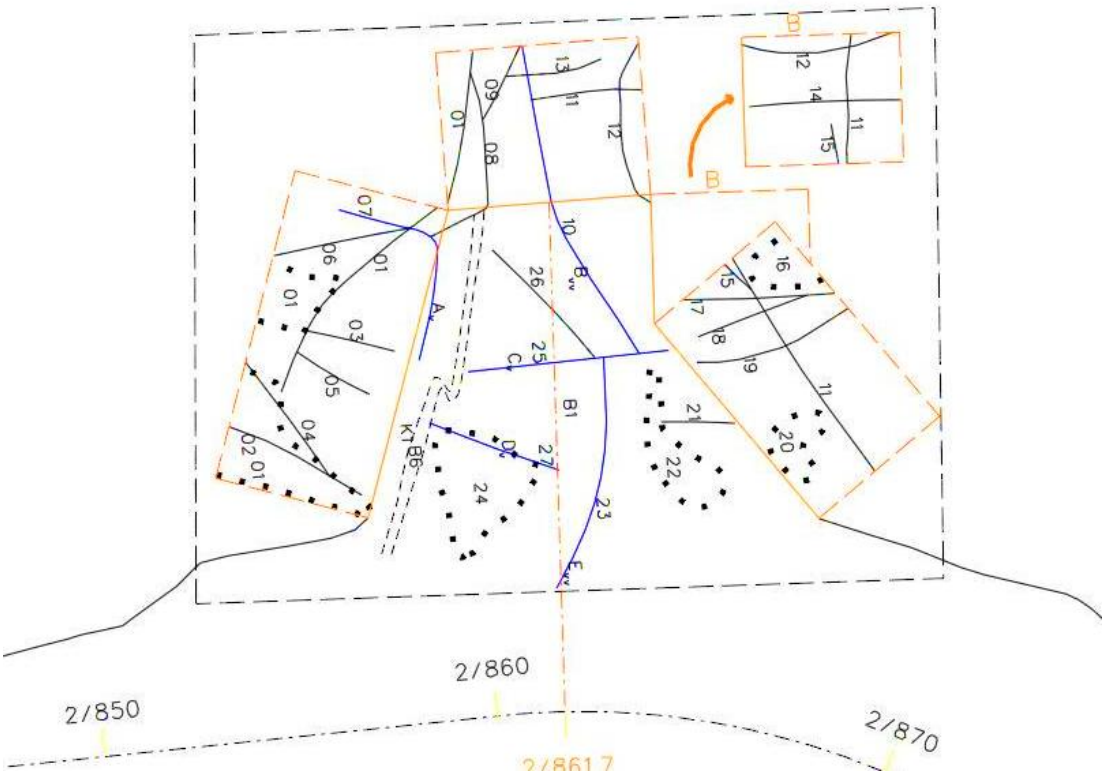

***Figure 2-5**. A schematic illustration of NASA2861A showing both the tunnel floor and walls. Blue lines illustrate water-bearing fractures whereas black lines illustrate dry fractures.*

2.2.2 Site characterisation

When NASA2861A was made available to the project it had already been mapped in a previous investigation and found to contain several water-bearing fractures (Figure 2-5) with water flows between 0.01 and 0.03 l/min. Based on these results and the requirements for the two experiments two pilot holes denominated KA2862G01 and KA2862G02 each with a diameter of 76 mm were drilled to a depth of about 4.1 meters each.

The cores were photographed both dry and wet and a core mapping protocol was prepared. A photograph of the wet cores from KA2862G02 representative also for KA2862G01 is shown in Figure 2-6.

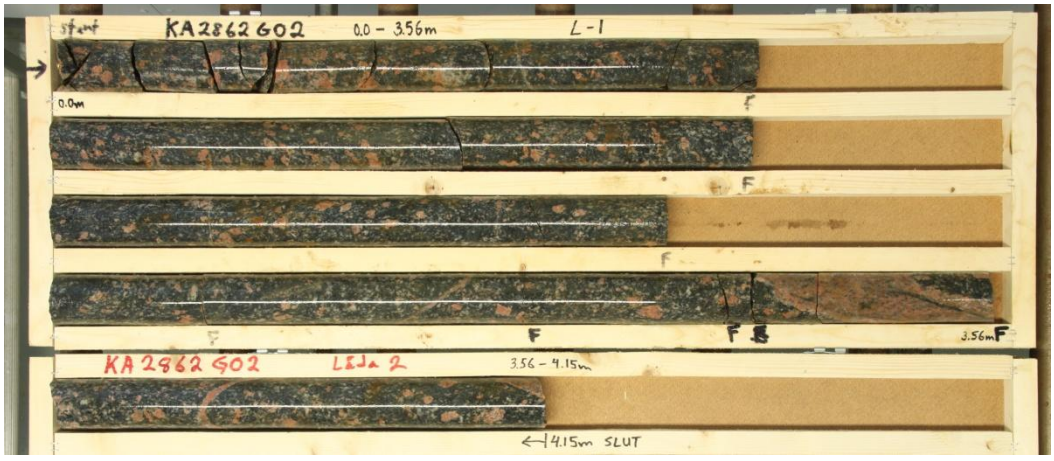

***Figure 2-6**. A photograph of the wet cores from the pilot hole KA2862G02 representative for both pilot holes in NASA2861A.*

Finally, the groundwater flow in the pilot holes was measured, Table 2-3.

Table 2-3. Groundwater flow in the pilot bore holes in NASA2861A.

Pilot bore hole	Water flow (l/min)
KA2862G01	0.01400
KA2862G02	0 (The hole was dry)

After measuring the groundwater flow, both pilot holes were over-cored to ∅ 350 mm and a final depth of about 4.0 meters.

The groundwater in the bedrock surrounding NASA2861 is characterised as deep saline with high concentrations of dissolved species and a low concentration of dissolved organic carbon, DOC. Table 2-4 presents average values for selected groundwater components from analyses carried out during the years 2015 to 2020.

Table 2-4. Groundwater composition in NASA 2861A

Component	Concentration (mg/l)
Cl^-	15790
SO_4^{2-}	597
Na^+	4120
Ca^{2+}	5699
DOC	1.28
pH	7.69

2.3 Site preparations

Site preparation comprised removing lose rock debris from the tunnel floor in the area around the installation hole and casting of the concrete base to which the lid should be secured after installation of the concrete cylinders, Figure 2-7.

Figure 2-7. *Casting of a concrete base.*

Just prior to installation of the concrete cylinders, sand was poured into the installation hole to adjust its depth but also to level its bottom, Figure 2-8.

Figure 2-8. *Levelling the bottom and measuring the depth of the installation hole.*

3 Experimental details

3.1 Overview of the experiments

Three experiments each comprising three concrete cylinders (Ø 300 mm and length 1000 mm each) were prepared and installed in TASR and NASA2861A during 2010 and 2011 respectively. Of the three concrete cylinders in each hole, one contained the metal objects covered in this report whereas the other two contained different types of organic materials. See (Mårtensson 2015) for more details.

Two of these experiments were installed in installation holes in TASR with good access to groundwater whereas the third was placed in a dry hole in NASA2861A to study the influence of the amount of available water on the degradation processes. A schematic illustration of an installed experiment and a concrete cylinder with metal objects is shown in Figure 3-1.

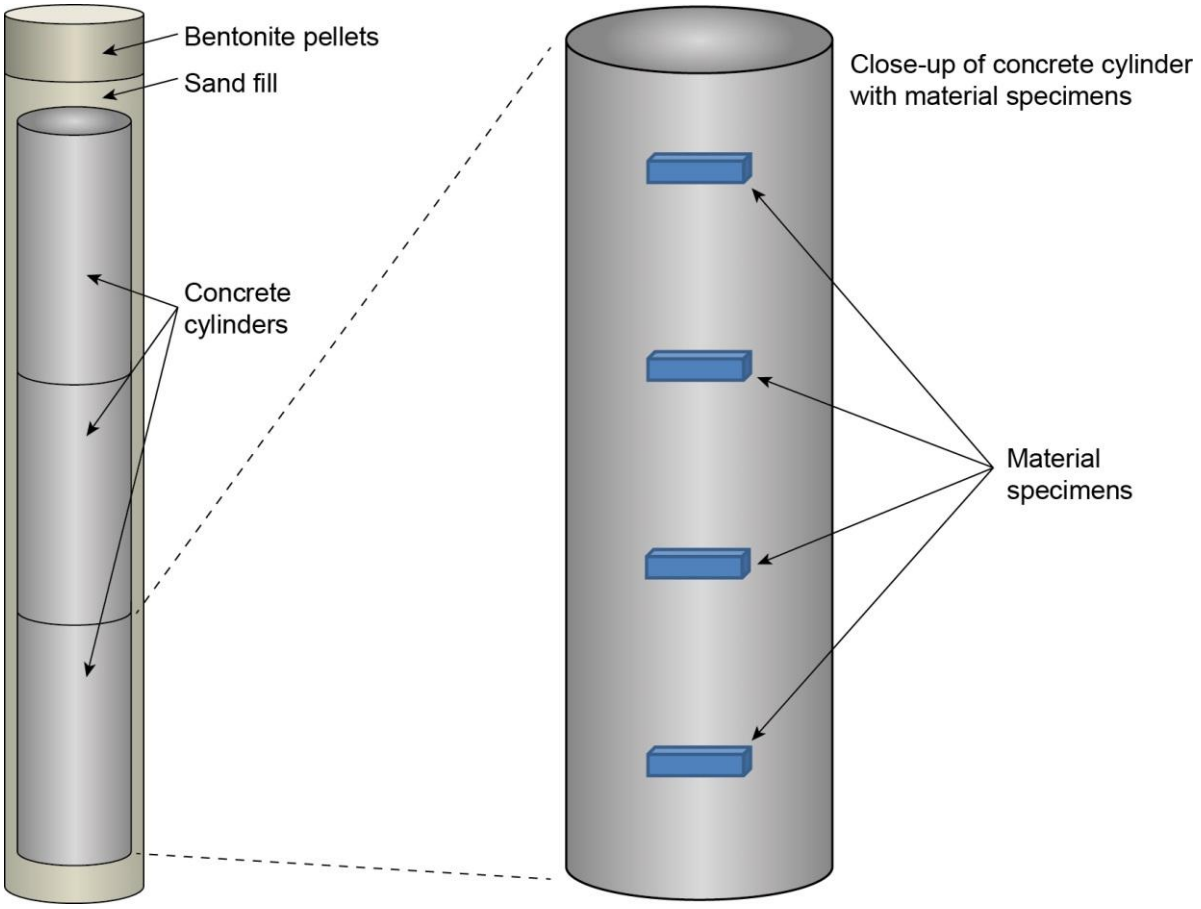

Figure 3-1. *A schematic illustration of an installed experiment (left illustration) and a concrete cylinder with metal objects – here denominated "Material specimens" (right illustration).*

3.2 Preparation of the concrete cylinders with metal objects

3.2.1 Materials used in the experiments

Concrete

The concrete cylinders were cast from a mixture of fibre grout 50 VF (Table 3-1) and water. The 50 VF grout was used for conditioning of waste for SFR at Ringhals Nuclear Power Plant and therefore selected for these experiments.

For each concrete cylinder, 156.0 kg of 50 VF dry mixture was mixed with 18.75 kg of water corresponding to a water–cement ratio of 0.42. The composition of the 50 VF is presented in Table 3-1 and the composition of the cement in Table 3-2. However, as mentioned in Mårtensson (2024) the composition of Degerhamn anläggningscement has varied a little over the years depending on variations in the composition of the raw material used for cement production.

Table 3-1. Composition of 50 VF Fibre grout[1]

Component	Type
Cement	Degerhamn Anläggningscement
Aggregates	Sand 0–4 mm
Fibres	Polypropylene, KRENIT®
Cement content:	7.2 kg / 25 kg dry product

Table 3-2. Composition of Degerhamn anläggningscement (Gaucher et al. 2005)

Component	Content (% by weight)
CaO	65.5
SiO_2	22.7
Al_2O_3	3.56
Fe_2O_3	4.32
MgO	0.45
K_2O	0.57
Na_2O	0.05
SO_3	2.07

Metal objects

The following types of metals were used in the long-term corrosion experiments:

- Zinc
- Aluminium
- Carbon steel
- Stainless steel SS2333

[1] SKBdoc 2128343 ver 1.0 (Internal document in Swedish.)

3.2.2 Preparations

Preparation of the metal objects

Each metal object was cut into a suitable size if required and weighed prior to casting of the concrete cylinders, Figure 3-2. Further information is given in Mårtensson (2015, Appendix B and C).

Figure 3-2*. Metal objects used in the long-term corrosion studies. Metal objects for concrete cylinders installed in TASR and NASA2821A to the left and right respectively.*

Casting of the concrete cylinders

The concrete cylinders were cast in ordinary sewage pipes with an inner diameter of 300 mm, Figure 3-3. In each concrete cylinder, a few metal objects (Figure 3-2) were placed at four different levels. For most of the metal objects this procedure worked well but some of them sank slightly in the wet and not yet hardened concrete. See (Mårtensson 2015, Appendix B and C) for details.

Figure 3-3. *The sewage pipes used as moulds for casting of the concrete cylinders (left image) and the interior of the mould during casting of concrete cylinders containing stainless-steel objects (right image).*

3.3 Installation of the concrete cylinders

The concrete cylinders were hoisted into the installation holes as shown in Figure 3-4 with the aid of a front loader truck.

After installation, the slit between the concrete cylinders and the bedrock in the wet holes was filled with sand. In the dry hole, the slit was instead filled with the same type of grout as was used for casting of the concrete cylinders, i.e. 50 VF. The purpose of this was mainly to centre the concrete cylinders in the installation hole but the sand also filled the purpose of distributing any water from the bedrock evenly within the installation hole.

Figure 3-4*. Installation of a concrete cylinder.*

After installation, sand was placed on top of the concrete cylinders in the wet installation holes. For the dry hole, this part was first partially filled with fibre grout 50 VF with sand on top.

After this, the part of the hole intersecting the interface between the concrete base shown in figure 3-4, central image and the bedrock was filled with bentonite pellets (Figure 3-5 left). The purpose of this was to seal the interface and prevent the intrusion of oxic (and potentially polluted) water from the tunnel floor into the deposition hole.

Finally, the hole was filled with sand up to its rim after which the lid was placed on top of the concrete base (Figure 3-5, right). The lid was then secured by means of two steel beams placed horizontally on top of the lid. The steel beams were finally secured in the bedrock by means of large bolts, Figure 3-6.

A summary of the experiments is presented in table 3-3. For further details, see Mårtensson (2015).

Figure 3-5*. Sealing and closure of a long-term corrosion experiment.*

Figure 3-6. *Installation of the long-term corrosion experiments in TASR completed*

Table 3-3. Installed concrete cylinders with metal objects (Mårtensson, 2015).

Concrete cylinder	Installation hole	Site	Installation year	Groundwater
I-1B	KR0014G01	TASR	2010	Wet
I-1A	KR0009G01	TASR	2010	Wet
I-1C	KA2862G02	NASA2861A	2011	Dry

4 Retrieval and sectioning of the concrete cylinders

This chapter shortly presents the methods used for retrieval and sectioning of the concrete cylinders done at the Äspö laboratory. Methods used for preparation of specimens for analyses are presented in Chapter 5.

4.1 Retrieval of the concrete cylinders

4.1.1 Concrete cylinders installed in wet holes

As a first step, the bolts holding the beams securing the lid were unscrewed and the concrete lid removed, Figure 4-1, left image. After that, the top sand was removed by means of a powerful vacuum cleaner. This was followed by removal of the concrete slab which separates sand and bentonite and finally, the bentonite was dug out. At this point, water was observed in the installation holes, Figure 4-1, right image, indicating that sufficient amounts of groundwater had been available to ensure water saturation of the concrete cylinders.

Figure 4-1. *The concrete lid is removed (left image). After removing the top seal, water was observed in the installation hole.*

The most laborious part of the retrieval turned out to be cleansing of the sand-filled slit. Attempts to lift the concrete cylinders without removing the sand were unsuccessful. Different methods were attempted to loosen up the sand and the work was both physically exhausting and rather time-consuming. However, eventually enough sand had been removed for the concrete cylinders to be hoisted up from the installation hole with the assistance of a front loader truck, Figures 4-2 to 4-4.

Figure 4-2*. Cleansing of the sand-filled slit between the concrete cylinders and the wall of the installation hole.*

Figure 4-3*. The concrete cylinder is being hoisted up from the installation hole.*

After the lift, the concrete cylinders were wrapped in plastic, placed on a pallet and transported up to the laboratory for sectioning, packaging and labelling, Figure 4-4.

Figure 4-4*. The concrete cylinders have been placed on a pallet for transport.*

4.1.2 Concrete cylinder installed in a nominally dry hole

Retrieval of concrete cylinder I-1C which was installed and grouted in a nominally dry installation hole was carried out by means of over-coring using a ∅ 350 mm core drill. This process did not proceed as smoothly as anticipated with occasional jamming of the drill and cracking of the concrete cylinder as a consequence.

Eventually, the concrete cylinder could be hoisted up of the hole but as shown in Figure 4-5 it was severely cracked.

Figure 4-5. *Concrete cylinder from the nominally dry hole in NASA2861A.*

4.2 Sectioning and packaging of the concrete cylinders

The concrete cylinders were each sectioned into four parts, Figure 4-6, each part containing objects of one type of metal and then wrapped in plastic prior to shipment, Figure 4-7. The different parts were numbered from 1 (top) to 4 (bottom).

Figure 4-6. *Sectioning of a concrete cylinder*

Figure 4-7*. The four parts of a concrete cylinder after sectioning and packaging.*

4.3 Retrieved concrete cylinders – summary

The concrete cylinders were retrieved and analysed at 5, 10 and 15 years after installation, respectively (Table 4-1). The fifth column shows the designation of the various samples used in the Results sections of this report.

Table-4-1. Details on installation and retrieval of the long-term corrosion experiments and original report in which the analyses were presented.

Concrete cylinder	Installation hole	Installed	Retrieved	Sample Id used in the Results sections*	Original report
I-1B	KR0014G01	2010	2015	5YW*-XX	Kalinowski (2015)
I-1A	KR0009G01	2010	2020	10YW-XX	Kalinowski (2020)
I-1C	KA2862G02	2011	2025	15YD-XX	Kalinowski (2026)

*-XX represents the type of metal object, see Table 4-2. ID reflects the age and saturation as years wet (YW) or years dry (YD), respectively.

Table 4-2. Designation used for the different metals in the results section in this report.

Metal object	XX*
Aluminium	Al
Zinc	Zn
Carbon steel	CS
Stainless steel	SS

*Refers to XX in the fifth column in Table 4-1.

5 Details of analysis

The following analyses were carried out:

- Measurement of the relative humidity in the concrete to verify that enough water had been present to sustain the corrosion process.
- Visual examination of the contact surface between the metal object and the concrete.
- Studies of the pore structure of the cement paste adjacent to the metal objects and presence of secondary minerals in the pores (thin section analysis).
- Microstructural analysis (scanning electrode microscopy, SEM)
- Analysis of compositional variations in the cement paste adjacent to the metal objects (SEM/ energy dispersive spectroscopy, EDS).
- Phase identification by means of X-ray diffraction (XRD).

5.1 Measurement of the relative humidity in concrete

For all parts of the concrete cylinders stored under wet conditions the surfaces appeared wet when the plastic cover was removed, indicating that the concrete had not dried out during transport and storage. However, Kalinowski (2026) does not provide information on the appearance of the concrete cylinder stored in the nominally dry hole.

Relative humidity (RH) measurements were carried out using an externally calibrated moisture meter of the model Testo 635 (CBI (Cement och Betonginstitutet/ Swedish Cement and Concrete Institute) calibration instrument). The temperature during the measurements was 20 °C.

For the measurements, a 100 mm deep hole with a diameter of 20 mm was drilled from flat surface of each part of the concrete cylinder, Figure 5-1, left image. The boreholes were cleaned and dried with compressed air and sealed with a rubber plug. The sensor was fitted with a rubber ring that prevented evaporation of moisture during the measurement period, Figure 5-1, right image.

Prior to RH measurements at a depth of 50 mm, the 50–100 mm borehole section was sealed with a wrapped rubber plug. All measurements were made at about 24 hours after that the RH sensor had been inserted into the borehole.

Figure 5-1*. Measurement of the relative humidity in one of the parts of a concrete cylinder (Kalinowski 2015).*

5.2 Visual examination of contact surfaces of the metal objects and the concrete

After extraction of the metal objects from the concrete cylinders, a visual examination of the contact surfaces of the metal objects and the concrete was carried out. The purpose of this was mainly to get a first visual impression of the extent of the corrosion process and degree of alterations of the concrete adjacent to the metal/concrete interface.

The embedded metal objects were separated from the concrete and the contact surfaces of the metal objects, and the concrete were examined visually using a stereo magnifying lens at a magnification of up to 65 times.

5.3 Structural analysis of the concrete using thin-section specimens

Structural analysis of the concrete at the metal/concrete interface was mainly focused on the pore structure of the cement paste in this part.

Specimens for structural analysis were prepared according to the scheme for so-called *Thin-section analysis*. Specimen preparation for such analysis includes impregnation of a very thin section of the concrete specimen with fluorescent epoxy to allow for a comparison of the capillary porosity of the concrete binder. Greater capillary porosity allows for the penetration of a greater amount of fluorescent epoxy and cement paste with high a porosity therefore appears brighter than cement paste with a low porosity. The specimens for thin-section analysis had the dimensions 45 × 25 mm and covered distances of 0–25 mm from the metal/concrete interface.

Structural analysis of the cement paste at the metal/concrete interface was conducted using a polarising microscope (magnification up to 1000 times). Light sources for ordinary light and UV light were used. See e.g. Figure 6-6 for examples of images recorded using these two light sources.

5.4 Microstructural analysis (SEM)

Microstructural analysis - also including analysis of the chemical composition of the cement paste and reaction products - was done using a scanning electron microscope (SEM) equipped with a backscattered electron detector (BSE detector) and energy dispersive X-ray spectroscope (EDS). All analysed areas in the cement paste were first checked with the BSE detector to avoid interferences caused by the aggregates.

The EDS analyses included elements with atomic number 11, i.e. sodium, and higher. The size of the analysed areas was 5 × 5 – 50 × 50 μm and the analysis time 20–30 Lsec (Live seconds). Calibration of EDS spectra was done against metallic Al and Cu. Quantification of elements from EDS spectra was calibrated against a standard cement paste with known composition (CBI reference sample SEM 0530). The results from the EDS analyses were converted to oxides and normalized to 100 wt.%.

5.5 Phase identification (X-ray diffraction, XRD)

Crystallographic analysis of crystalline precipitates at the metal/concrete interface was performed using X-ray powder diffraction (powder XRD). Identification of diffraction peaks was performed via database search: JCPDS-ICDD, Joint Committee on Powder Diffraction Standards-International Centre for Diffraction Data, 1994.

6 Long-term studies of zinc corrosion – Results

6.1 Concrete relative humidity

The relative humidity in the parts of the concrete cylinders containing the zinc objects is presented in Table 6-1.

Table 6-1 shows that RH was high and sufficient to sustain a corrosion process regardless of whether they were stored under wet or nominally dry conditions.

Table 6-1. Relative humidity in the section of the concrete cylinders containing the zinc objects.

Sample	RH (%)	
	50 mm below surface	100 mm below surface
5YW-Zn	82	96
10YW-Zn	Not measured	93
15YD-Zn	Not measured	97 – 99*

*Relative humidity was only measured on the part of the concrete cylinder that contained the carbon-steel objects, but this is assessed to be representative also for the other parts of that concrete cylinder.

6.2 Visual examination

6.2.1 Surface of the metal objects

Figure 6-1 shows that the surfaces of the zinc objects are oxidised and dull and covered in greyish/beige precipitates regardless of duration of the experiment and storage conditions. However, signs of extensive corrosion are not observed.

In some places, the surface is coated with a mixture of cement paste, ettringite and precipitates of colourless crystals. The latter were identified by EDS analysis as zinc hydroxide ($Zn(OH)_2$) and calcium hydroxide ($Ca(OH)_2$), Section 6.3. The thickness of the surface layers was only up to about 100 μm for zinc objects stored under wet conditions for ten years. See also Section 6.3.

Figure 6-1. *Surface of the zinc object from samples 5YW-Zn (Top left image), 10YW-Zn (Top right image) and 15YD-Zn (lower image).*

6.2.2 Concrete surface at the metal/concrete interface

From visual examination, the surface of the concrete in contact with the zinc object mainly consists of hardened cement paste and corrosion products were not visually observed. Figure 6-2 shows a concrete imprint from a zinc object from sample 10YW-Zn which is representative for all zinc objects.

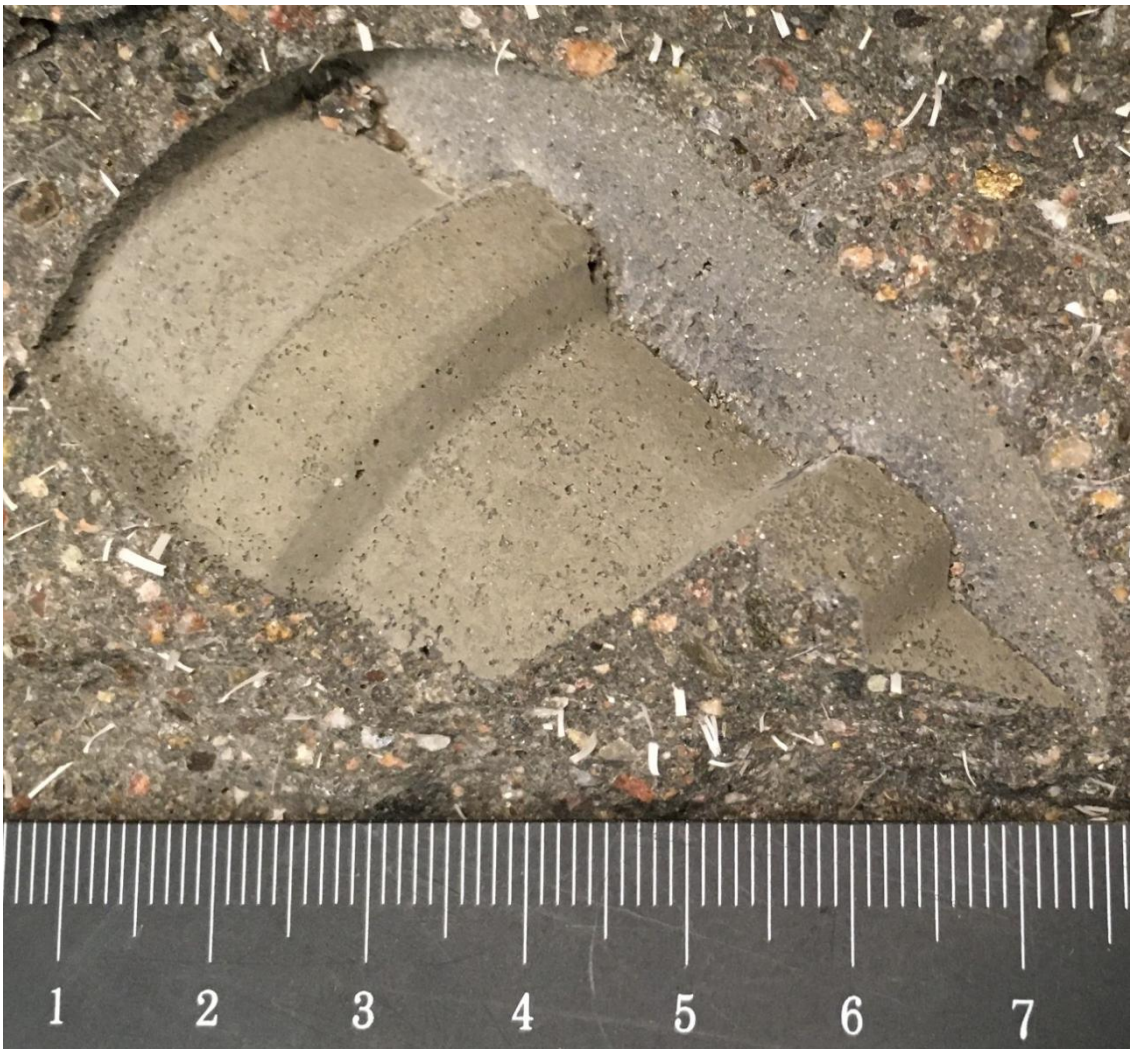

Figure 6-2. *A concrete imprint of a zinc object from sample 10YW-Zn.*

6.3 Structural analyses of the metal/concrete interface

Microstructural analysis (SEM) revealed the presence of pores and precipitates in the concrete surface at the metal/concrete interface (Figure 6-3) but also the presence of colourless euhedral (well-formed) crystals in the cement paste in this part, Figure 6-4. Analysis of the chemical composition of the crystals shown in Figure 6-4 showed that they consist of Zn and Ca compounds, either in the form of Zn and Ca hydroxide in solid solution or as intergrown crystals of Zn and Ca hydroxides.

No distinct zinc compounds were observed in the cement paste at a distance greater than 100 μm from the metal surface.

At greater distances from the metal/concrete interface (up to about 500 μm), zinc was observed in the form of sub microscopic compounds or as zinc ions bound to components of the cement paste such as the calcium silicate gel. Some of the zinc ions may also be present in aqueous solution that fills the capillary porosity in the cement paste (pore solutions) but this has not been confirmed. See Section 6.4 for further information on ion diffusion in the cement paste.

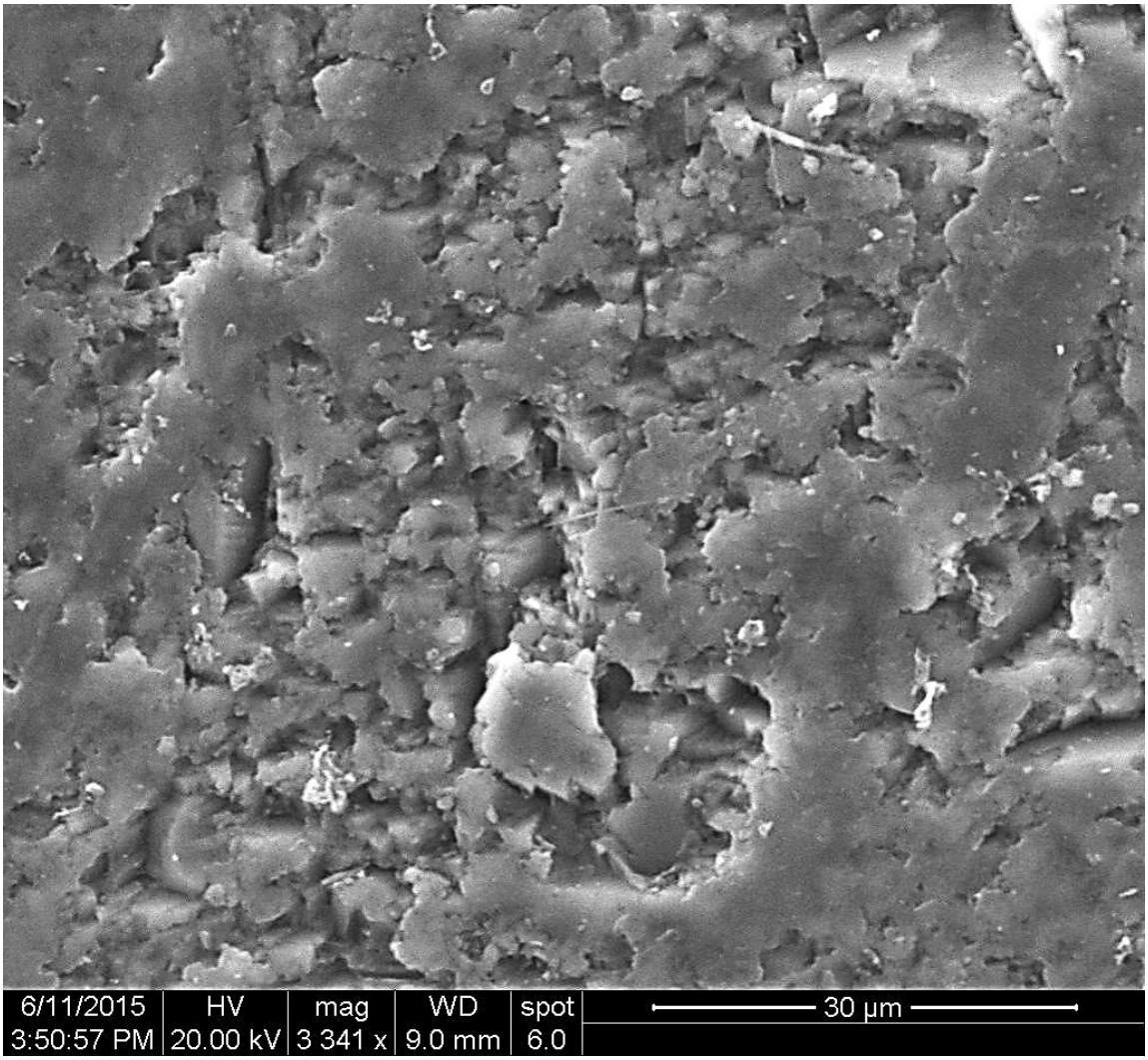

Figure 6-3. *Surface of the concrete at the zinc/concrete interface, SEM/BSE-detector. (Kalinowski 2015)*

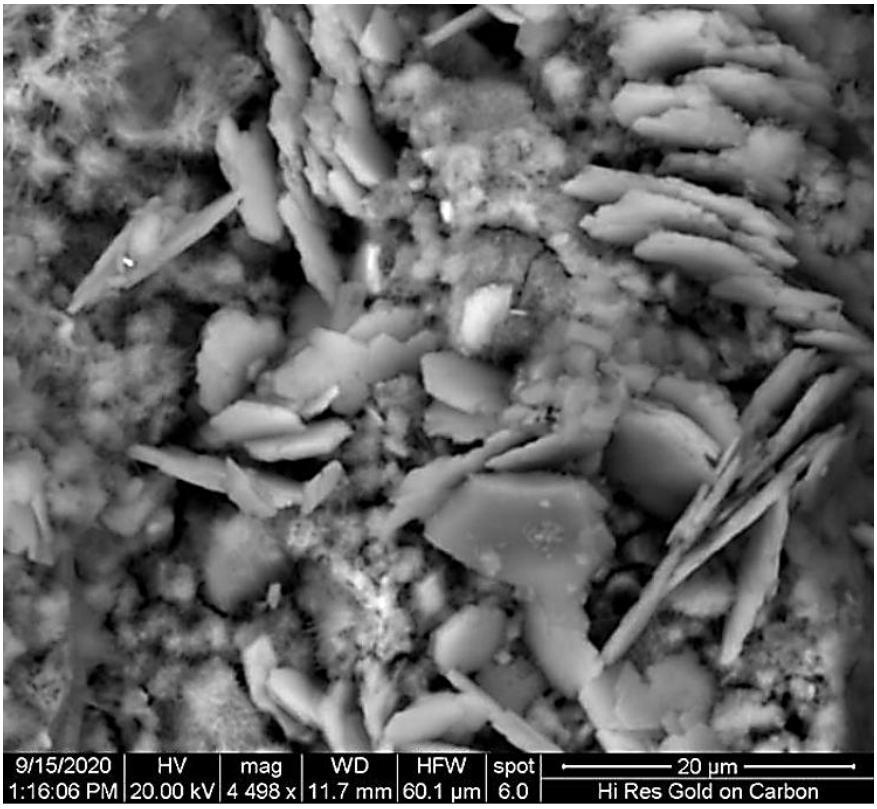

Figure 6-4. *Crystals fond at 0 – 60 µm from the zinc surface, SEM/BSE detector (Kalinowski 2020)*

Figure 6-5*. A single grain used to analyse the chemical composition of the grains identified on the surface of the zinc object, SEM/BSE detector. (Kalinowski 2015)*

Structural analysis (thin-section analysis) shows that there is a 0–1 mm wide zone in the cement paste at the metal/concrete interface with a slightly increased capillary porosity as well as occasional larger pores or blisters, Figures 6-6 and 6-7.

In addition, there is a small number of microcracks with widths up to about 0.01 mm in a zone extending up to 2 mm from the metal surface. These cracks were either caused by drying shrinkage of the cement paste during hardening of the concrete cylinder or during preparation of the thin-section specimens.

The crystals of zinc hydroxide and calcium hydroxide that were observed on parts of the metal surface were not observed in the thin-section specimens.

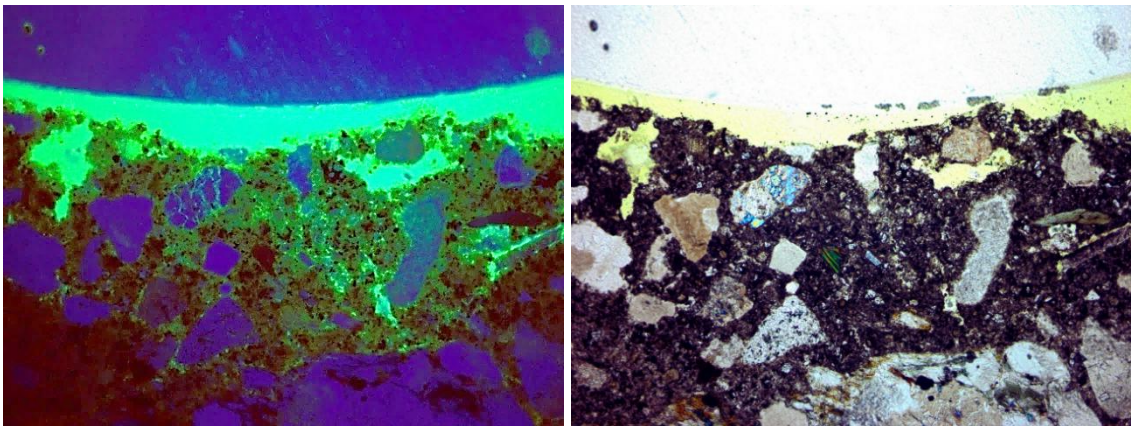

Figure 6-6. *Photographs of a thin-section specimen of the concrete part at the zinc/concrete interface of sample 5YW-Zn in ultraviolet light (left) and polarized light (right). The images show an area of the specimen with a width of 6.7 mm (Kalinowski 2015).*

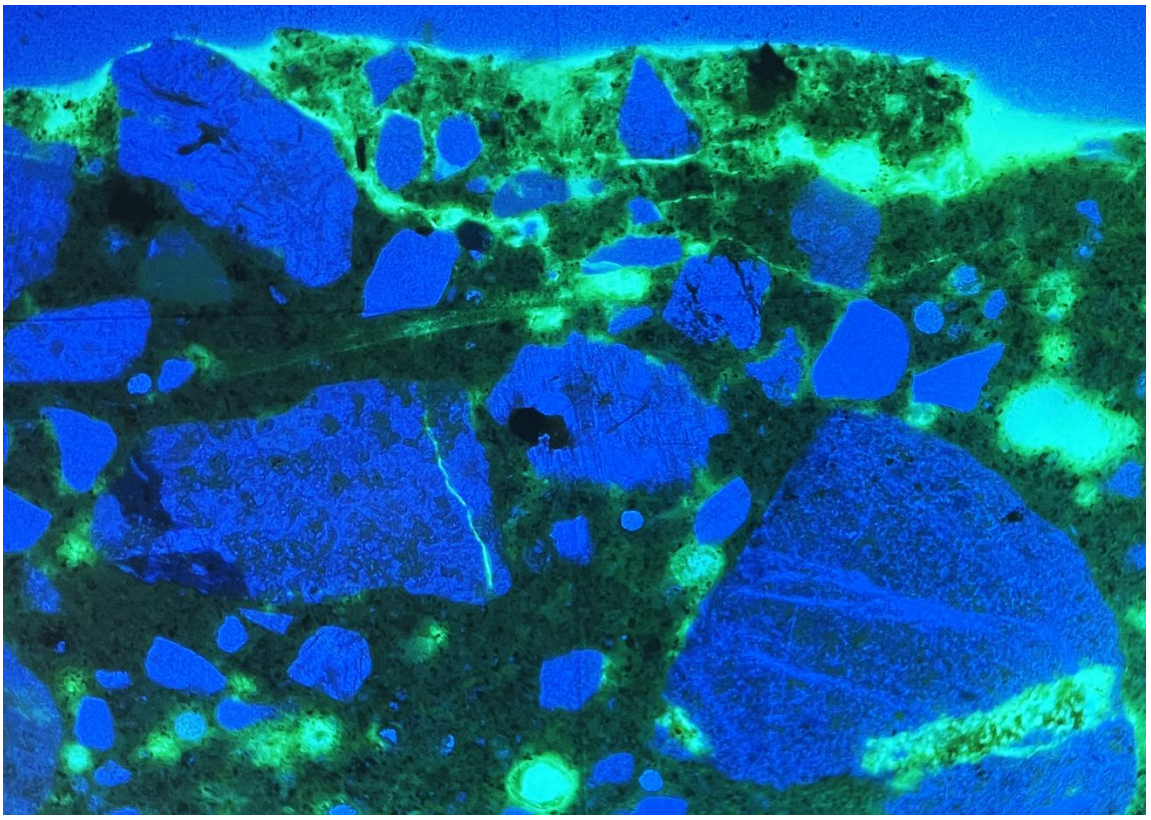

Figure 6-7. *Photograph of a thin-section specimen of the concrete part at the zinc/concrete interface of sample 15YD-Zn in ultraviolet light. The images show an area of the specimen with a width of 6.7 mm (Kalinowski 2026).*

6.4 Zinc concentration profile in the cement paste

Slightly increased levels of zinc were found up to about 0.5 mm from the metal/concrete interface with somewhat lower values after ten years than after five, and the 15-years values fall in between (Figure 6-8).

When comparing the zinc concentration profiles with the other results presented in this chapter it is assessed that the zinc observed in the EDS analyses mainly originates from the corrosion products found on the metal surface or in the pores adjacent to the zinc objects rather than as dissolved zinc ions in the porewater of the cement paste. This assessment is also supported by the fact that the concentration profiles for the three different samples are similar regardless of their (nominal) storage conditions and time of storage. If there had been significant amounts of dissolved zinc, the assessment is that the concentration profile would have changed to a greater extent over time than is now observed.

It can thus be concluded that the long-term zinc corrosion process as well as the transport of zinc ions in the concrete matrix during the cause of the experiment is very slow in this environment. In addition, these studies show that the process practically halts once the layer of corrosion products has formed on the metal surface or in the pore system of the cement matrix. This is also supported by the findings by Herting and Odnevall (2021) who showed a rapidly decreasing zinc corrosion rate already during the first couple of months after experiment start.

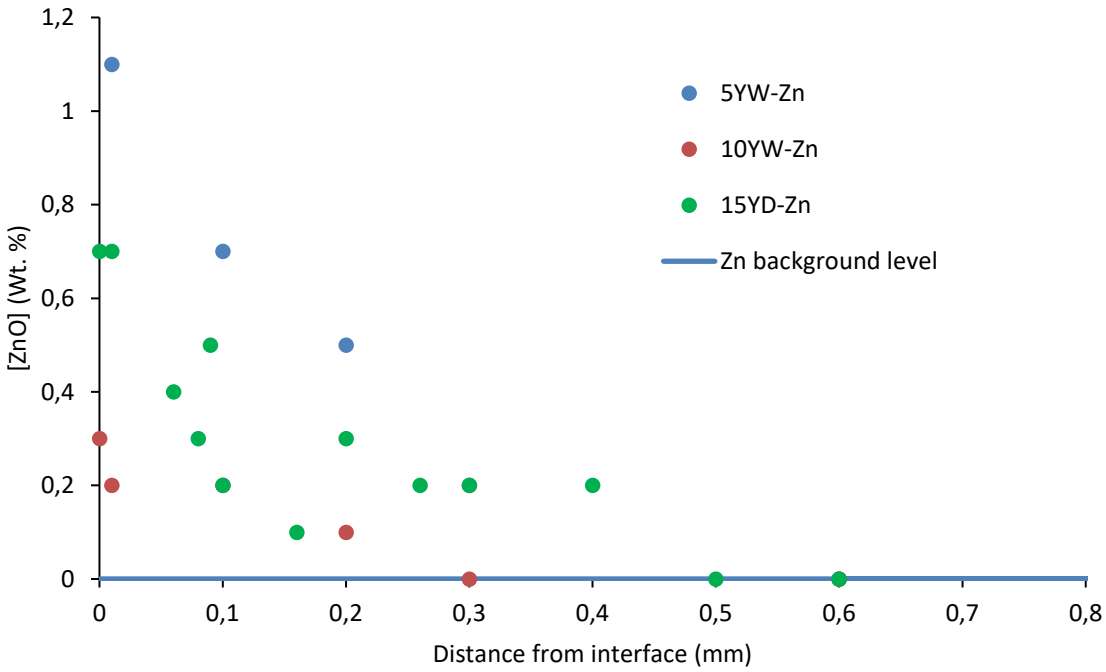

Figure 6-8. *Zinc (as ZnO) concentration profiles in the concrete adjacent to the zinc objects for samples 5YW-Zn, 10YW-Zn and 15YD-Zn. Average data from the EDS-analyses also including additional elements are presented in Appendix 1.*

6.5 Summary of the observations

In this chapter, the results from long-term zinc corrosion experiments carried out over a period of up to 15 years at the Äspö hard rock laboratory have been presented.

The following observations have been made.

- The long-term zinc corrosion rate is low, and no support for the assumed corrosion rate of one millimetre per year (SKB 2008) has been found in this study. Instead, the corrosion process seems to halt once the concrete has hardened and a layer of corrosion products has formed on the metal surface or in the pore system of the cement paste even though the relative humidity in the concrete is sufficient to sustain the corrosion process.
- The pores observed in the cement paste at the metal/concrete interface were probably formed due to hydrogen evolution caused by the reaction between the metal object and the alkaline pore solutions of the cement paste already during casting of the concrete cylinders. In comparison with aluminium, the porous zone was somewhat smaller.
- Close to the metal/concrete interface, zinc prevails as colourless euhedral (well-formed) crystals $Zn(OH)_2$ or as $(Ca, Zn)(OH)_2$.
- At greater distances from the metal/concrete interface (up to about 500 μm), zinc prevails either as sub-microscopic compounds or as zinc ions bound to cement paste components such as calcium silicate gel. Some of the zinc ions may also be present in the aqueous solution that fills the capillary porosity in the cement paste (pore solutions), but this has not been confirmed.
- When comparing the zinc concentration profiles with the other results presented in this chapter it is assessed that the zinc observed in the EDS analyses mainly originates from the corrosion products found on the metal surface or in the pores adjacent to the zinc objects rather than as dissolved zinc ions in the porewater of the cement paste. This assessment is also supported by the fact that the concentration profiles för the three different samples are similar regardless of their (nominal) storage conditions and time of storage. If there had been significant amounts of dissolved zinc, the assessment is that the concentration profile would have changed to a greater extent over time than is now observed.

7 Long-term studies of aluminium corrosion – Results

Unexpectedly, the aluminium objects in the concrete cylinder stored for 15 years could not be found when conducting the preparations prior to the analyses. The reason for this is unclear but the most plausible explanation is that the metal objects were left in the installation hole when the concrete cylinder cracked during retrieval. For that reason, this chapter can only present the results from studies of concrete embedded aluminium objects stored for five and ten years under wet conditions respectively.

7.1 Concrete relative humidity

The relative humidity in the parts of the concrete cylinders containing the aluminium objects is presented in Table 7-1.

Table 7-1 shows that RH for the two concrete cylinders stored under wet conditions was high and sufficient to sustain a corrosion process.

Table 7-1. Relative humidity in the concrete cylinders containing the aluminium objects

Sample	RH (%)	
	50 mm below surface	**100 mm below surface**
5YW-Al	89	97
10YW-Al	Not measured	92

7.2 Visual examination

7.2.1 Surface of the metal objects

The surface of the aluminium object is oxidised, dark grey-to-black and dull, Figure 7-1, but signs of extensive corrosion is not observed. The metal objects are embedded in a layer of reaction products consisting of a thin inner dark layer and a thicker outer, white-to-beige layer.

The inner layer consists mainly of aluminium hydroxide and is firmly attached to the metal surface while the outer layer is porous and consists of reaction products mixed with cement paste. The outer layer is mainly found in the pores in the concrete.

Figure 7-1. *Surface of the aluminium object 5YW-Al (top) and 10YW-Al (bottom).*

7.2.2 Concrete surface at the metal/concrete interface

In the concrete at the metal/concrete interface, a thin, dark (dark grey/black) crust of reaction products with an average and a maximum thickness of about 150 µm and one mm respectively is observed, Figure 7-2.

Between this crust and the unaffected concrete there is a light (grey/beige) and porous layer of reaction products with a general thickness of 0.5–2 mm, Figure 7-2. In addition, also some pores filled with reaction products which extend further into the concrete were observed. Overall, the cement porosity was significantly larger in the cement paste in contact with aluminium than with zinc which indicates a more vigorous reaction between aluminium and the alkaline pore solution than for zinc.

Chemical and crystallographic analysis (EDS/SEM and XRD) indicate that the reaction products are mainly composed of aluminium hydroxide and a smaller amount of crystallised hydrated calcium aluminium silicates, Section 7.3.

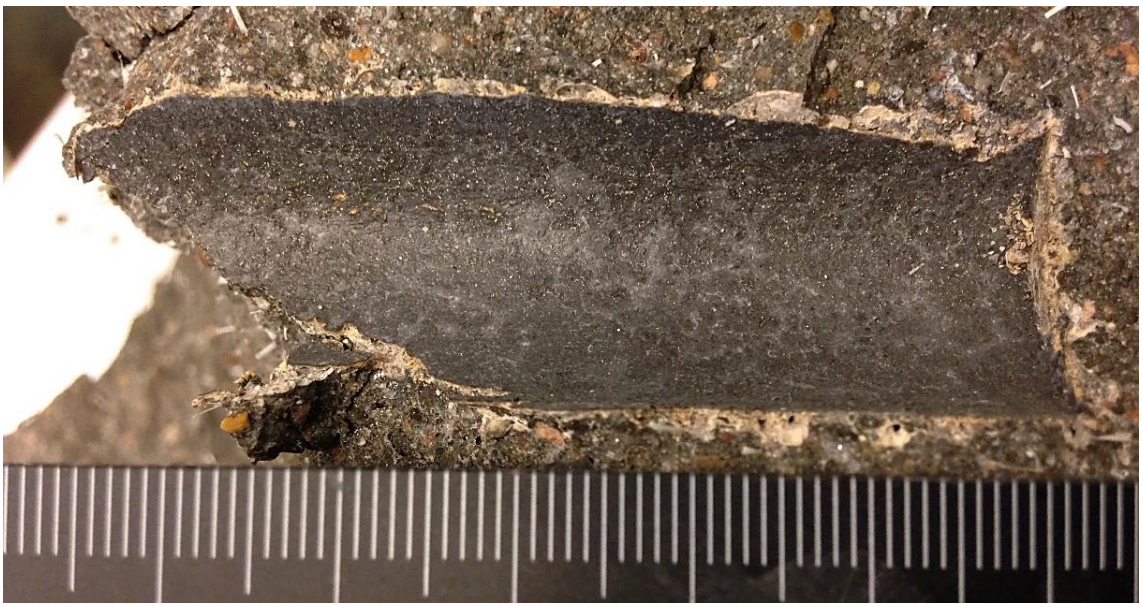

Figure 7-2. *A concrete imprint of an aluminium object from sample 10YW-Al. (Kalinowski 2020).*

7.3 Structural analyses of the metal/concrete interface

Microstructural investigations (SEM) of the concrete at the metal/concrete interface revealed a layer of reaction products consisting mainly of aluminium hydroxide. In addition, a porous layer in the concrete comprising pores filled with a mixture of partly crystalline reaction products and cement paste was observed, Figure 7-3. These observations agree well with the findings presented in the previous section.

The reaction products and the areas in which the cement paste is mixed with the reaction products have a higher "capillary porosity" than the cement paste in general. Thin-section analyses showed that these areas extend up to a maximum of about 2 mm from the metal/concrete interface, Figures 7-6 and 7-7.

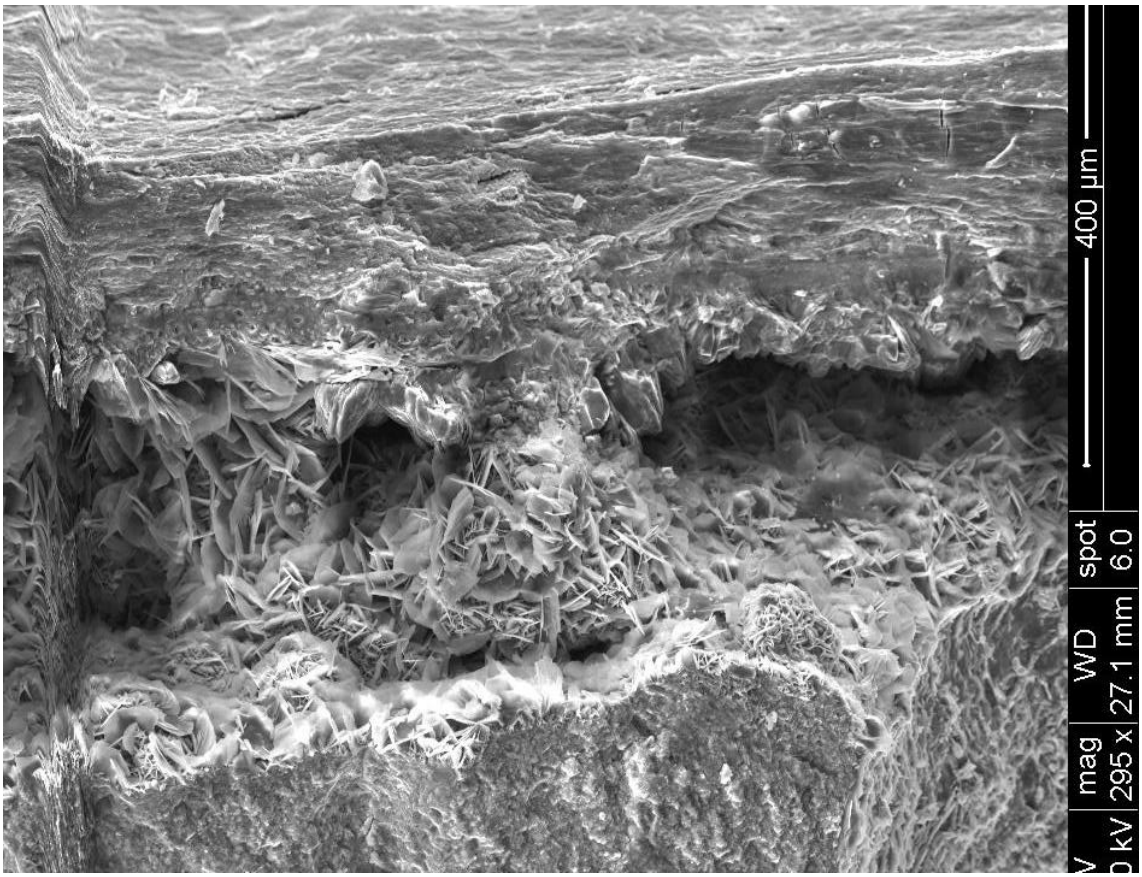

Figure 7-3. *Cross-section of sample 5YW-Al showing pores filled with crystalline reaction products in the cement paste at the metal/concrete interface. The image was taken with a BSE detector. The contact surface with the metal object faces upwards in the image. (Kalinowski, 2015)*

The precipitates found in the pores at the metal/concrete interface were analysed by means of powder XRD and the diffractograms are shown in Figure 7-4 and 7-5. Comparison with reference diffraction patterns show good agreement with aluminium hydroxide, Figure 7-4. Several peaks that did not match with aluminium hydroxide were identified as originating from hydrated calcium-aluminium-silicate compounds, Figure 7-5.

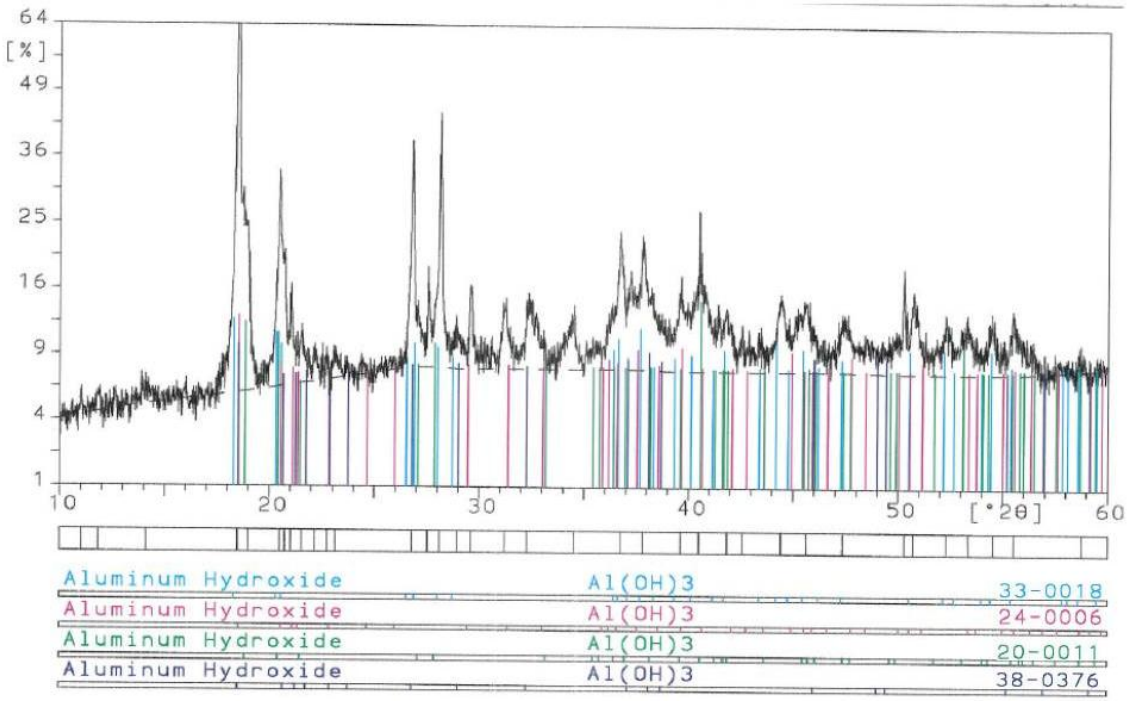

Figure 7-4. *X-ray diffractogram from precipitates from the aluminium/concrete interface for sample 5YW-Al. Reference lines representing aluminium hydroxide.*

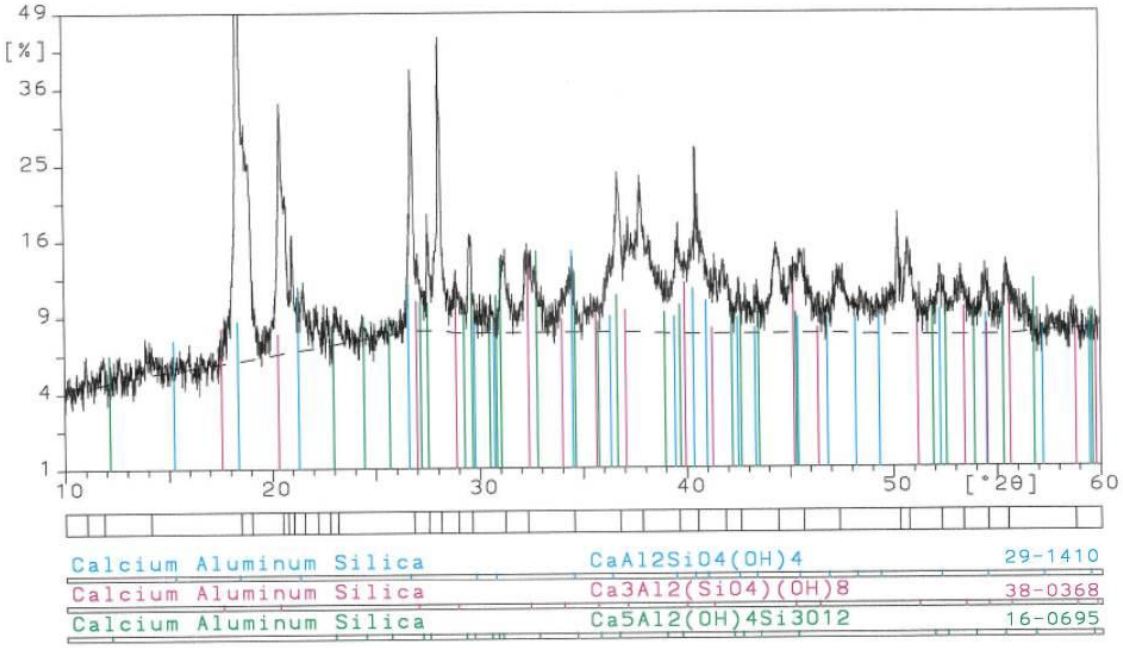

Figure 7-5. *X-ray diffractogram from precipitates from the aluminium/concrete interface for sample 5YW-Al. Reference lines representing calcium-aluminium-silicates.*

Structural analyses of thin-section specimens confirmed the presence of a porous zone close to the metal/concrete interface, Figures 7-6 and 7-7. The pores – visible as bright green areas – had a maximum length and width of about five and one millimetre respectively.

In all, the number and dimensions of the pores were basically the same in samples 5YW-Al and 10YW-Al. This implies that the concrete porosity in the metal/concrete interface were formed during casting of the concrete cylinders and not during the storage in the bedrock.

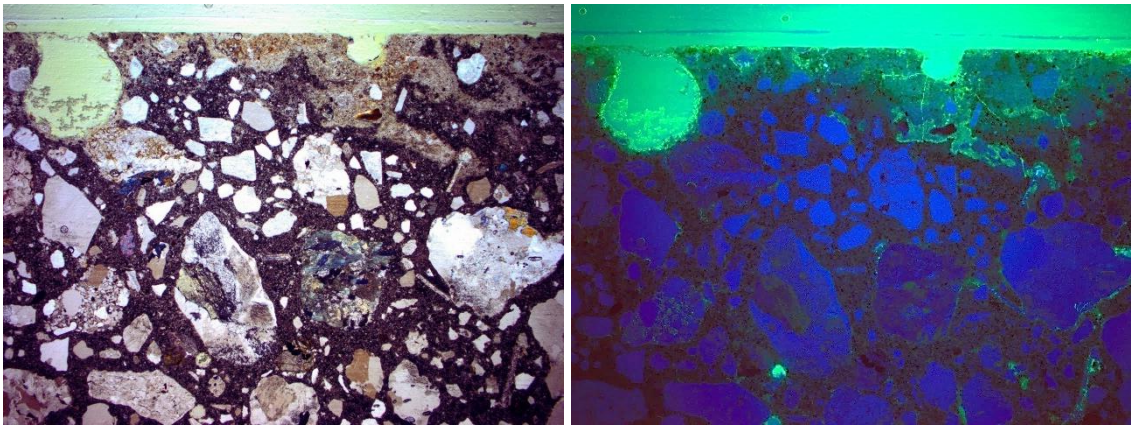

Figure 7-6. *Images of a thin-section specimen from sample 5YW-Al. The images show an area of the specimen with a width of 6.7 mm. Polarised light (left) and ultraviolet light (right)*

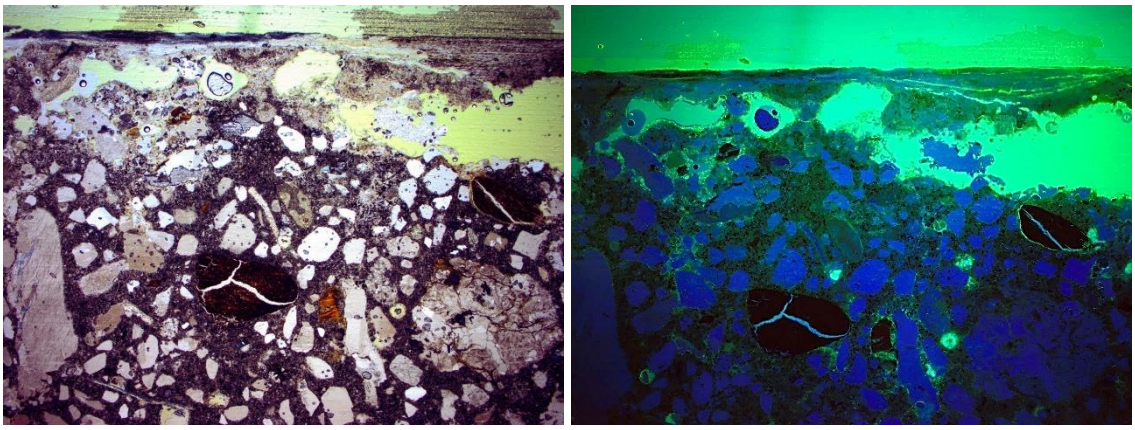

Figure 7-7. *Images of a thin-section specimen from sample 5YW-Al. The images show an area of the specimen with a width of 6.7 mm. Polarised light (left) and ultraviolet light (right).*

Structural analysis (thin-section specimens) also revealed the presence of several microcracks in the vicinity of the metal/concrete interface, Figure 7-8.

The width and length of these cracks were generally in the region of up to 0.02 mm and 5 mm respectively. In the area closest to the metal/concrete interface the microcracks were somewhat narrower with widths in the region of < 0.01 mm.

The origin of the microcracks is a bit uncertain with volume changes in connection with precipitation of reaction products or drying shrinkage of the concrete as the most probable mechanisms but some cracks may also have been formed during preparation of the thin-section specimen.

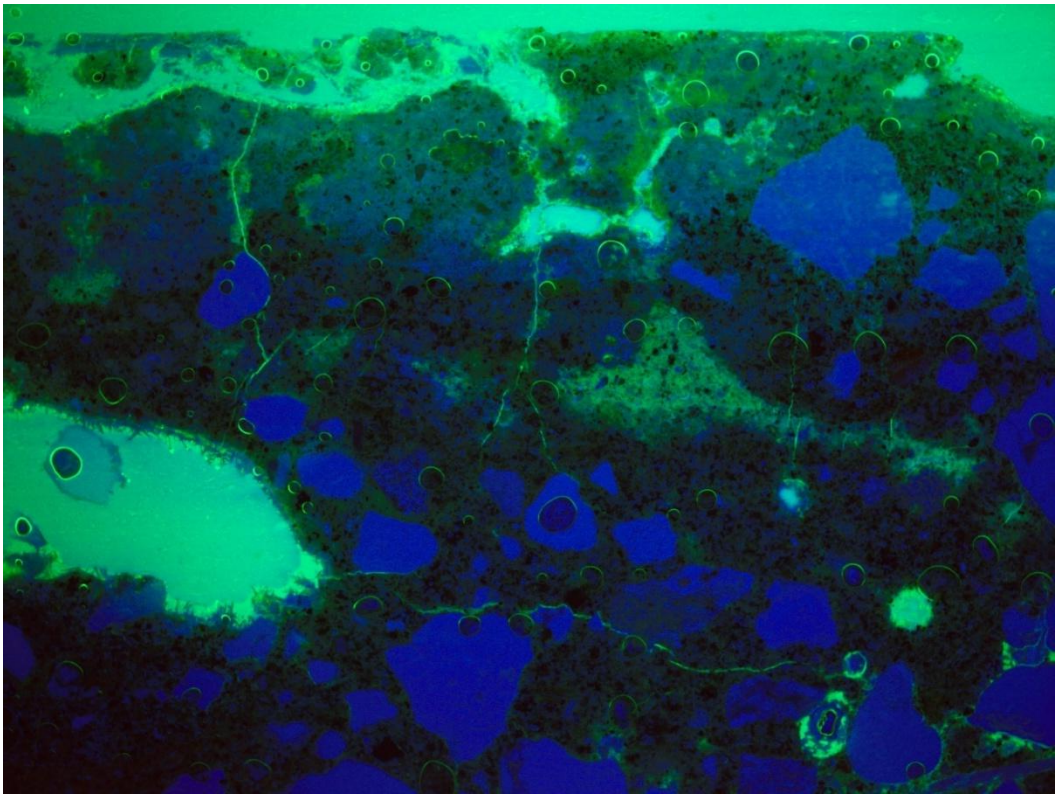

Figure 7-8. *Image of a thin-section specimen from the aluminium/concrete interface of sample 5YW-Al in ultraviolet light showing microcracks as thin green lines. The image shows an area of the specimen with a width of 6.7 mm.*

7.4 Aluminium concentration profile in the cement paste

For samples 5YW-Al and 10YW-Al, significant levels of aluminium were found in up to one millimetre from the metal/concrete interface, Figure 7-9. However, in some positions, increased levels were also found up to about 1.5 mm from the metal/concrete interface but in these parts only spot wise.

From about two mm from the interface, the average aluminium concentration was basically the same as the background level, of 4.5 ± 0.3 wt.%, even though somewhat higher in isolated parts. These variations may be caused by local variations in the composition of the cement paste but also by the pore size variations at the interface and cannot with certainty be attributed to diffusion of Al ions in the porewater of the cement paste.

As with zinc, when comparing the aluminium concentration profiles with the other results presented in this chapter it is assessed that the aluminium observed in the EDS analyses mainly originates from the corrosion products found on the metal surface or in the pores adjacent to the aluminium objects rather than as dissolved aluminium ions in the porewater of the cement paste. This assessment is also supported by the fact that the concentration profiles för the two samples are similar regardless of their time of storage. If there had been significant amounts of dissolved aluminium, the assessment is that the concentration profile would have changed to a greater extent over time than is now observed.

It can thus be concluded that the long-term aluminium corrosion process as well as the transport of aluminium ions in the concrete matrix is very slow in this environment. In addition, these studies show that the process practically halts once the layer of corrosion products has formed on the metal surface or in the pore system of the cement matrix. This is also supported by the findings by Herting and Odnevall (2021) who showed a rapidly decreasing aluminium corrosion rate already during the first couple of months after experiment start.

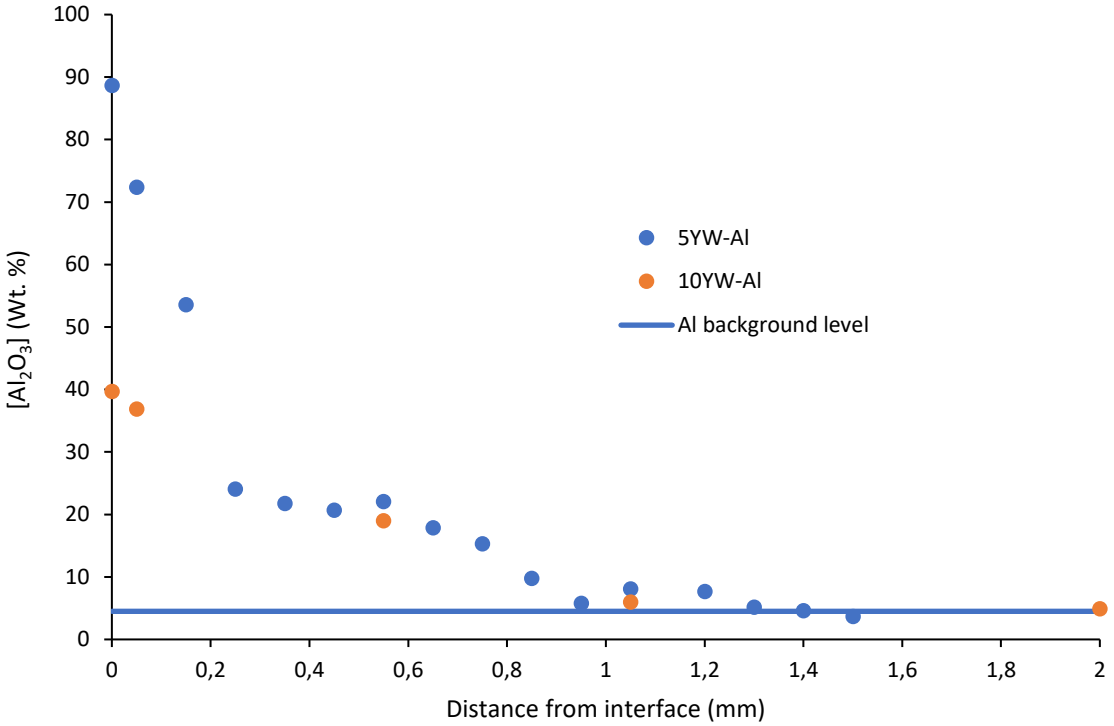

Figure 7-9. *Aluminium (as Al_2O_3) concentration profiles in the concrete adjacent to the aluminium objects for samples 5YW-Al and 10YW- Al. Average data from the EDS-analyses also including additional elements are presented in Appendix 1.*

7.5 Summary of the observations

In this chapter, the results from long-term aluminium corrosion studies carried out over a period of up to 10 years at the Äspö hard rock laboratory have been presented.

The following observations were made.

- The long-term aluminium corrosion rate is low, and no support for the assumed corrosion rate of one millimetre per year (SKB 2008) has been found in this study. Instead, the corrosion process seems to halt once a sufficiently thick and homogeneous layer of corrosion products has formed on the metal surface or in the pore system of the cement paste even though the relative humidity in the concrete is sufficient to sustain the corrosion process. As the first observation was made after five years exposure, these experiments do not allow for an accurate assessment on at which point in time this occurred. As a comparison, Herting and Odnevall (2021) Herting and Odnevall (2021) observed a rapidly decreasing aluminium corrosion rate already during the first couple of months after experiment start.
- The pores observed in the cement paste at the metal/concrete interface were probably formed due to hydrogen evolution caused by the reaction between the metal and the alkaline pore solutions of the cement paste already during casting of the concrete cylinders. These pores - the size and extent of which are clearly larger than for the cement paste in contact areas with metallic zinc - were later filled with reaction products.
- The layer of reaction products comprises an inner somewhat denser layer with an average thickness of about 150 µm and an outer layer which comprises a porous mixture of reaction products and cement paste with a thickness of about 0.5–1 mm. However, in isolated parts larger protrusions were also observed.
- Chemical and crystallographic analyses of the reaction products with SEM/EDS and XRD indicate that the reaction products are mainly composed of aluminium hydroxide and a smaller amount of crystallized hydrated calcium aluminium silicates.

- As with zinc, when comparing the zinc concentration profiles with the other results presented in this chapter it is assessed that the aluminium observed in the EDS analyses mainly originates from the corrosion products found on the metal surface or in the pores adjacent to the aluminium objects rather than as dissolved aluminium ions in the porewater of the cement paste. This assessment is also supported by the fact that the concentration profiles för the two samples are similar regardless of their time of storage.

8 Long-term studies of carbon-steel corrosion - Results

8.1 Concrete relative humidity

The relative humidity in the sections of the concrete cylinders containing the carbon-steel objects is presented in Table 8-1.

Table 8-1 shows that RH in all concrete cylinders was high and sufficient to sustain a corrosion process regardless of whether they were stored under wet or nominally dry conditions.

Table 8-1. Relative humidity in the concrete cylinders containing the carbon-steel objects

Sample	RH (%)	
	50 mm below surface	100 mm below surface
5YW-CS	92	97
10YW-CS	No data	92
15YD-CS		97–99

8.2 Visual examination

8.2.1 Surface of the metal objects

The reinforcement bars were coated with a thin layer of reddish-brown iron hydroxide corrosion products similar to that of the bars prior to casting of the concrete cylinders (Figure 3-2) for all samples regardless of storage conditions and time of storage, Figure 8-1.

Figure 8-1. *Photograph of carbon-steel objects 5YW-CS (with concrete imprint) (top) and 15YD-CS (bottom).*

8.2.2 Concrete surface at the metal/concrete interface

The surface of the concrete imprints of the reinforcement bars mainly consists of "cement skin" with spots of reddish-brown iron hydroxide/corrosion products, Figure 8-2, but no signs of extensive corrosion are observed. The origin and time of formation of the corrosion products have not been determined. However, it cannot be excluded that they originate from corrosion products already present at the reinforcement bars at the time of casting of the concrete cylinder and which have attached to the concrete.

Figure 8-2. *Concrete imprints of carbon-steel objects for samples 10YW-CS (top) and 15YD-CS (bottom).*

8.3 Structural analyses of the metal/concrete interface

As noted in Section 8.2, the amount of corrosion products on the concrete at the metal/concrete interface was minute in all carbon-steel objects. Instead, the surface of the concrete at the metal/concrete interface is a bit porous (Figure 8-3) with some of the pores partially filled with crystals of portlandite ($Ca(OH)_2$), Figure 8-4.

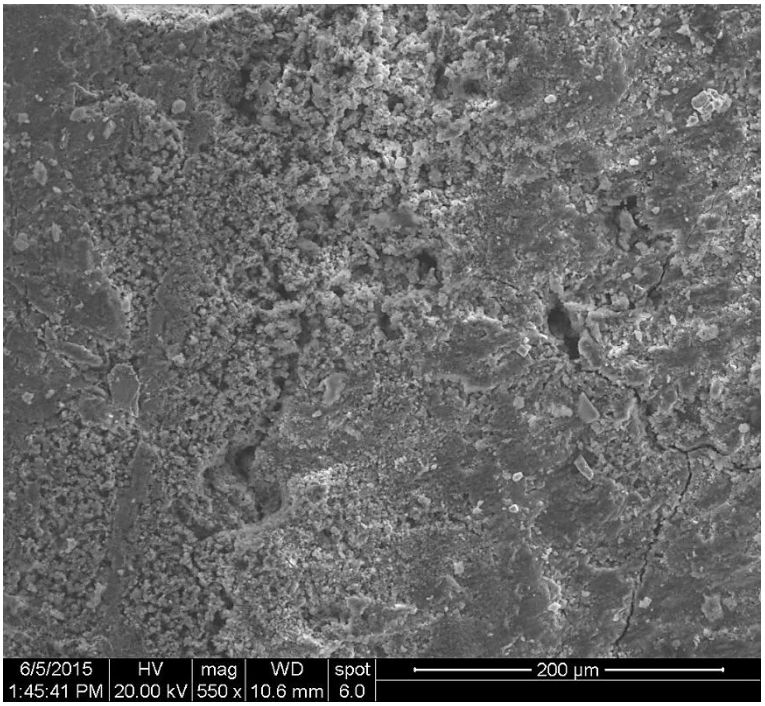

Figure 8-3. *Surface of the concrete at the carbon-steel/concrete interface in sample 5YW-CS, SEM/BSE-detector (Kalinowski 2015).*

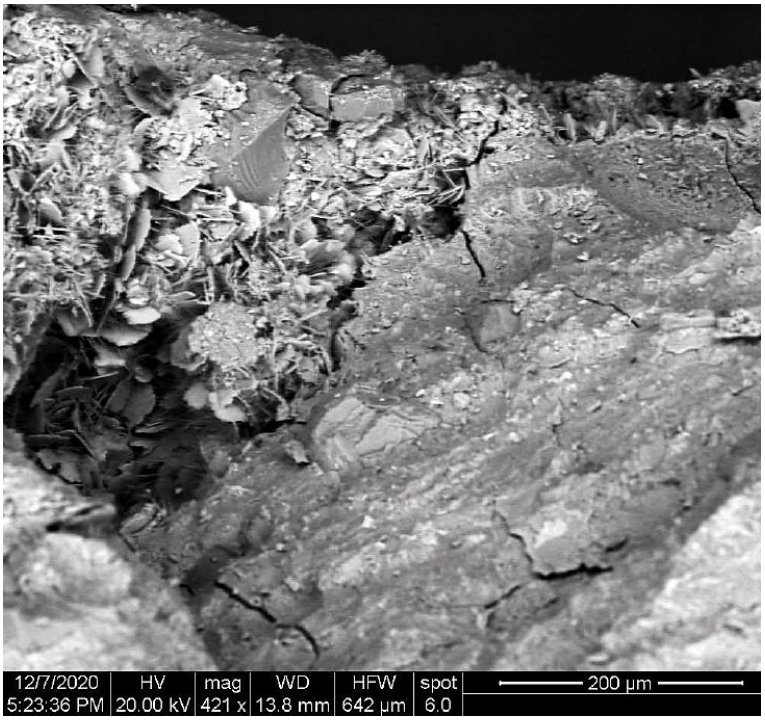

Figure 8-4. *SEM/BSE image showing crystals of portlandite in a concrete pore at the metal/concrete interface in sample 10YW-CS (Kalinowski 2020).*

Structural analyses of thin-section specimens show that there is a slight increase in capillary porosity in a region between 0.02–0.5 mm from the metal/concrete interface, Figure 8-5. There is also a small number of microcracks with widths of a maximum of 0.01 mm in the region up to two millimetres from the metal surface, Figure 8-6. The origin of the microcracks is a bit uncertain with volume changes in connection with precipitation of reaction products or drying shrinkage of the concrete as the most probable mechanisms but some cracks may also have been formed during preparation of the thin-section specimens.

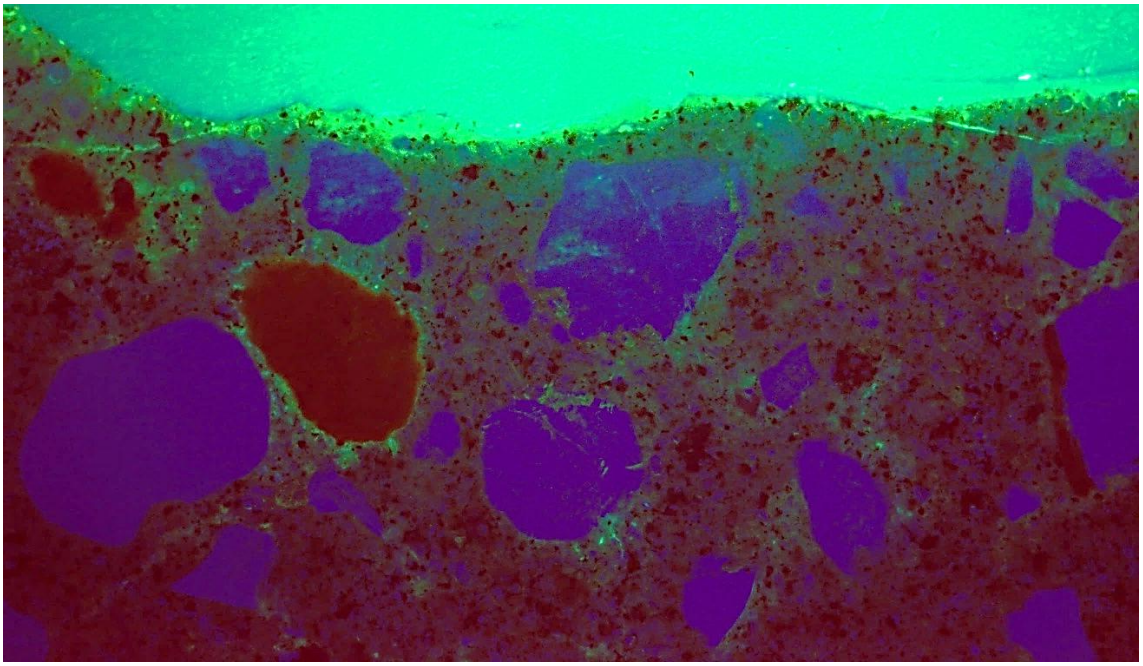

Figure 8-5. *Photograph of a thin-section specimen of sample 5YW-CS in ultraviolet light. The image shows the metal/concrete interface in the top of the image and covers an area with a width of 1.4 mm.*

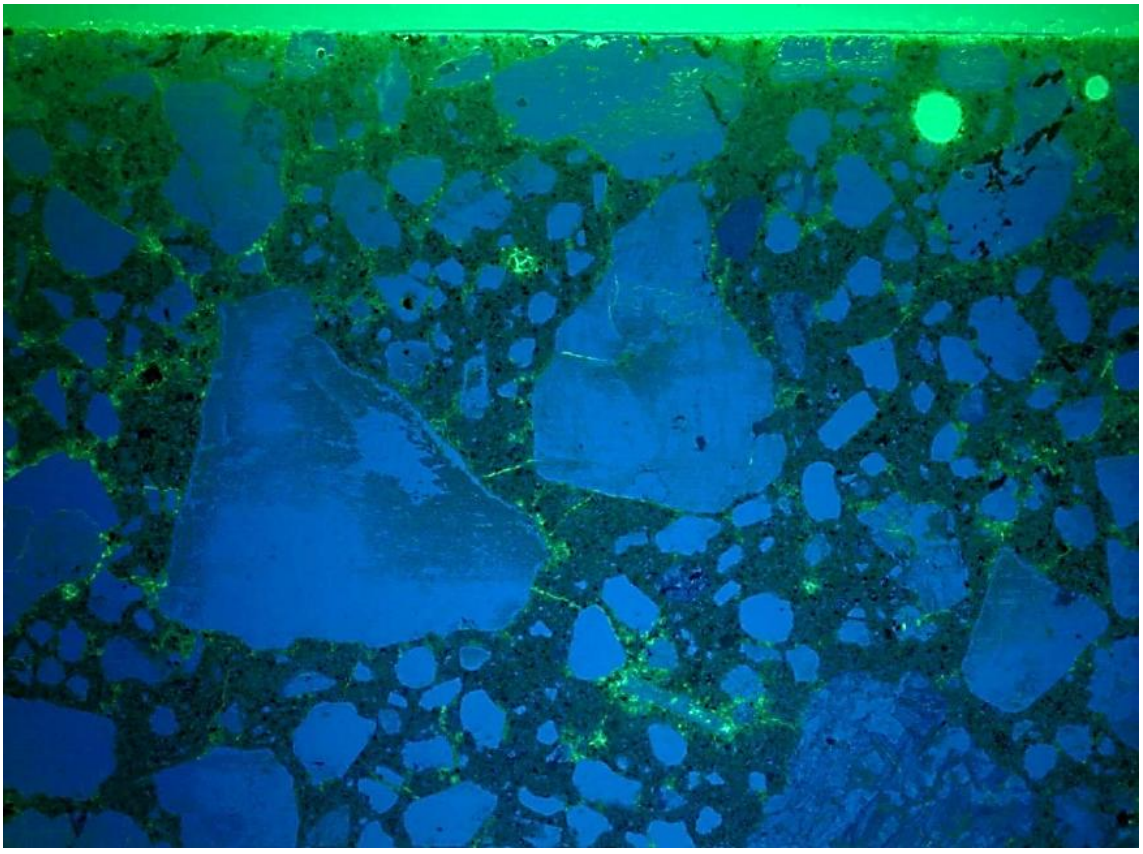

Figure 8-6. *Photograph of a thin-section specimen of sample 10YW-CS in ultraviolet light. The image shows the metal/concrete interface in the top of the image and covers an area with a width of 6.7 mm.*

8.4 Iron concentration profile in the cement paste

SEM/EDS analyses of the concrete close to the metal/concrete interface showed only minutely increased levels of iron (reported as Fe_2O_3) in the studied samples, Figure 8-7. However, already in the regions 0–0.03 mm, 0.05 mm (0.03–0.06 mm) and 0.5 mm from the metal/concrete interface the average Fe_2O_3 levels were basically the same as the background level of the cement paste of 4.0 ± 0.3 wt.% indicating a very low corrosion rate.

These findings agree with those presented in Sections 8.2.1 and 8.2.2 where only small spots of iron hydroxide corrosion products were observed on the surface of the concrete imprint.

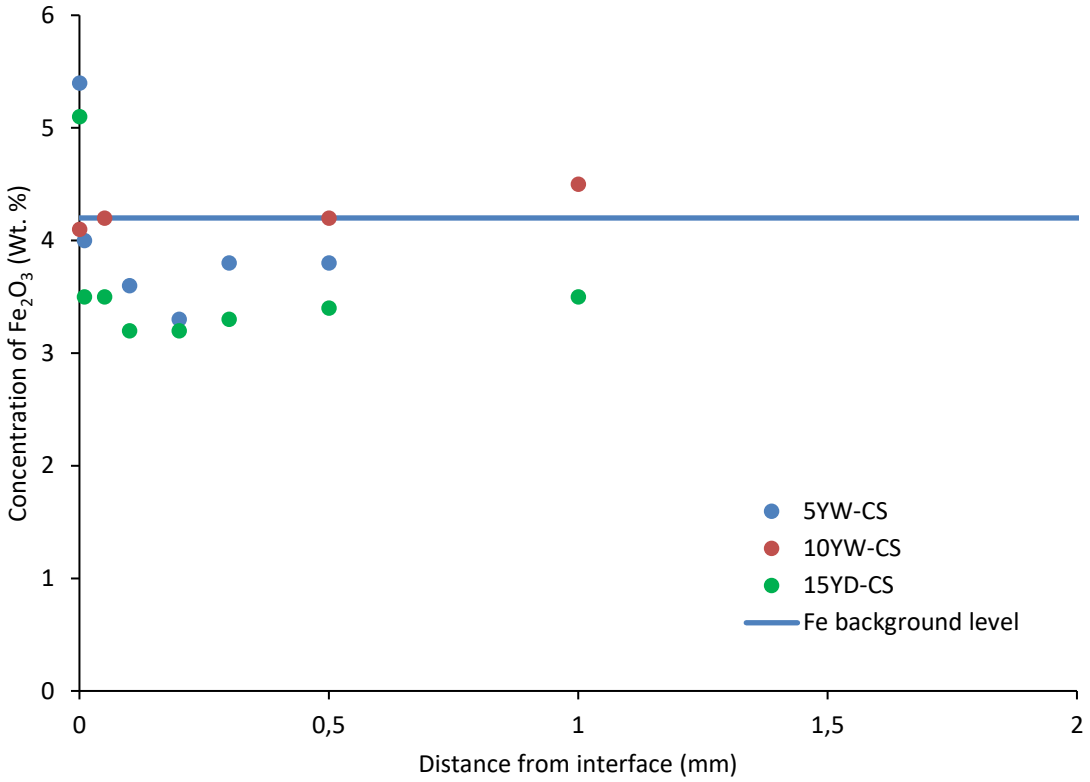

Figure 8-7. *Iron (as Fe_2O_3) concentration profiles in the concrete adjacent to the carbon-steel objects in samples 5YW-CS, 10YW- CS and 15YD- CS. Average data from the EDS-analyses also including additional elements are presented in Appendix 1.*

8.5 Summary of the observations

In this chapter, the results from long-term carbon-steel corrosion studies carried out over a period of up to 15 years at the Äspö hard rock laboratory have been presented.

The following observations have been made:

- No signs of corrosion of the carbon-steel objects were observed for any of the samples regardless of storage time and conditions.
- The appearance of the carbon-steel objects after completion of the experiments was the same as when the concrete cylinders were prepared.
- The iron concentration in the cement paste close to the metal/concrete interface was basically the same as the background level in the cement paste or lower.
- Only a slight increase of the porosity of the cement paste at the metal/concrete interface was observed. This differs significantly from the observations made for the aluminium and zinc objects where large pores filled with reaction products were found in this region. This type of small pores is commonly observed close the concrete aggregates and cannot unequivocally be attributed to reactions between the cement paste and the carbon-steel objects.

9 Long-term studies of stainless-steel corrosion – Results

9.1 Concrete relative humidity

The relative humidity in the parts of the concrete cylinders containing the stainless-steel objects is presented in Table 9-1.

Table 9-1 shows that RH in all of the concrete cylinders was high and sufficient to sustain a corrosion process regardless of whether they were stored under wet or nominally dry conditions.

Table 9-1. Relative humidity in the concrete cylinders containing the stainless-steel objects

Sample	RH (%)	
	50 mm below surface	100 mm below surface
5YW-SS	89	97
10YW-SS	No data	93
15YD-SS		97–99*

*Relative humidity was only measured on the part of the concrete cylinder that contained the carbon-steel objects, but this is assessed to be representative also for the other parts of that concrete cylinder.

9.2 Visual examination

9.2.1 Surface of the metal object

The stainless-steel objects showed no signs of corrosion, and the surfaces were uncorroded and had a metallic sheen, Figure 9-1. However, on some objects, small amounts of calcium hydroxide adhered to the metal surface, Figure 9-1, top left image.

Figure 9-1. *Surface of the stainless-steel objects from samples 5YW-SS (top left), 10YW-SS (top right) and 15YD-SS (lower).*

9.2.2 Concrete surface at the metal/concrete interface

The contact surfaces appear to consist of cement skin with patchy precipitations of calcium hydroxide (portlandite).

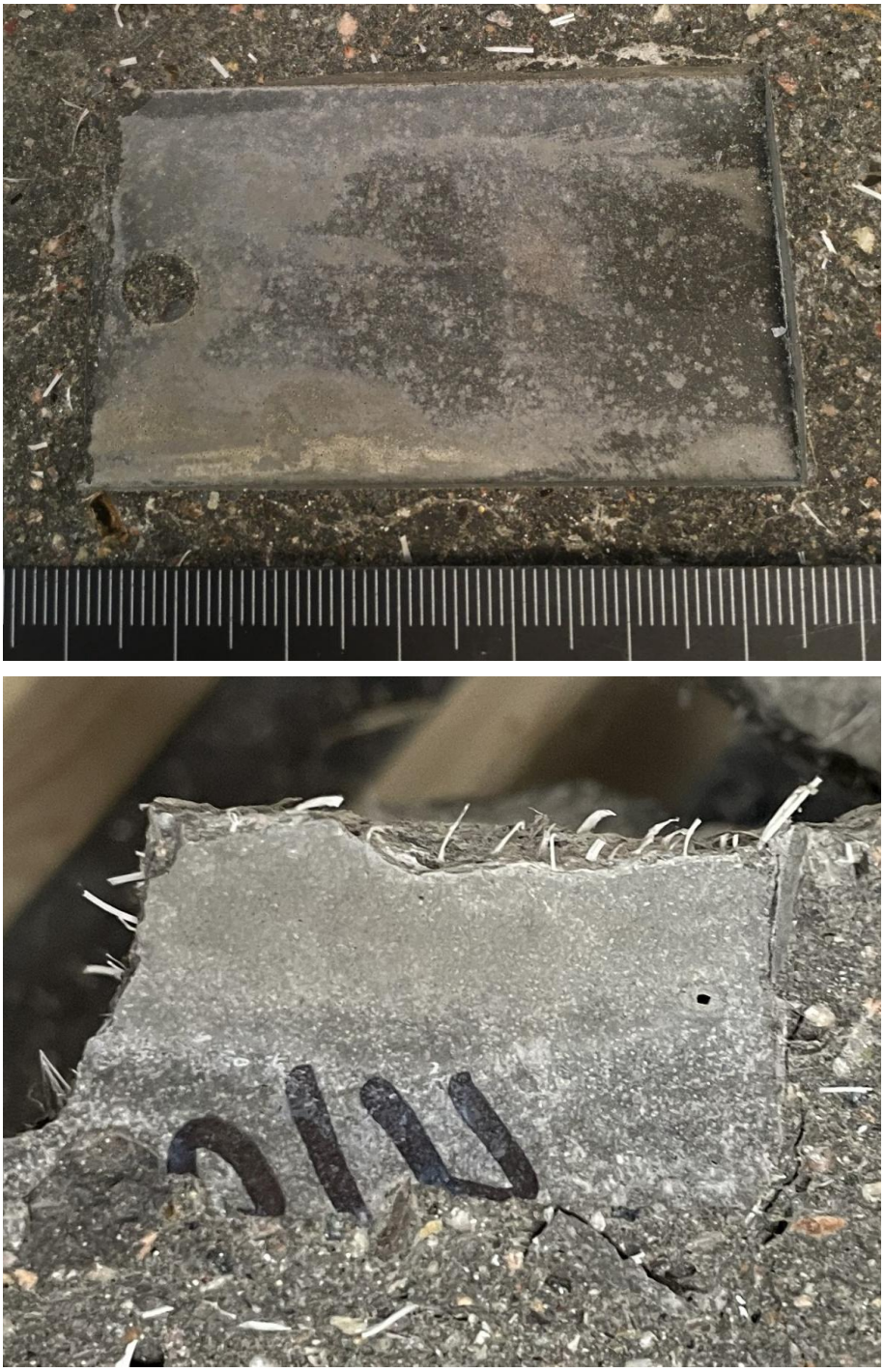

Figure 9-2. *Concrete imprints from stainless-steel objects from samples 10YW-SS (top) and 15YD-SS (bottom).*

9.3 Structural analyses of the metal/concrete interface

As indicated in Figure 9-2, some precipitation had occurred on the surface of the metal objects as well as on the concrete imprints. SEM/BSE studies (Figure 9-3) show that the precipitates in some parts were crystalline and probably at least partially consisting of portlandite ($Ca(OH)_2$).

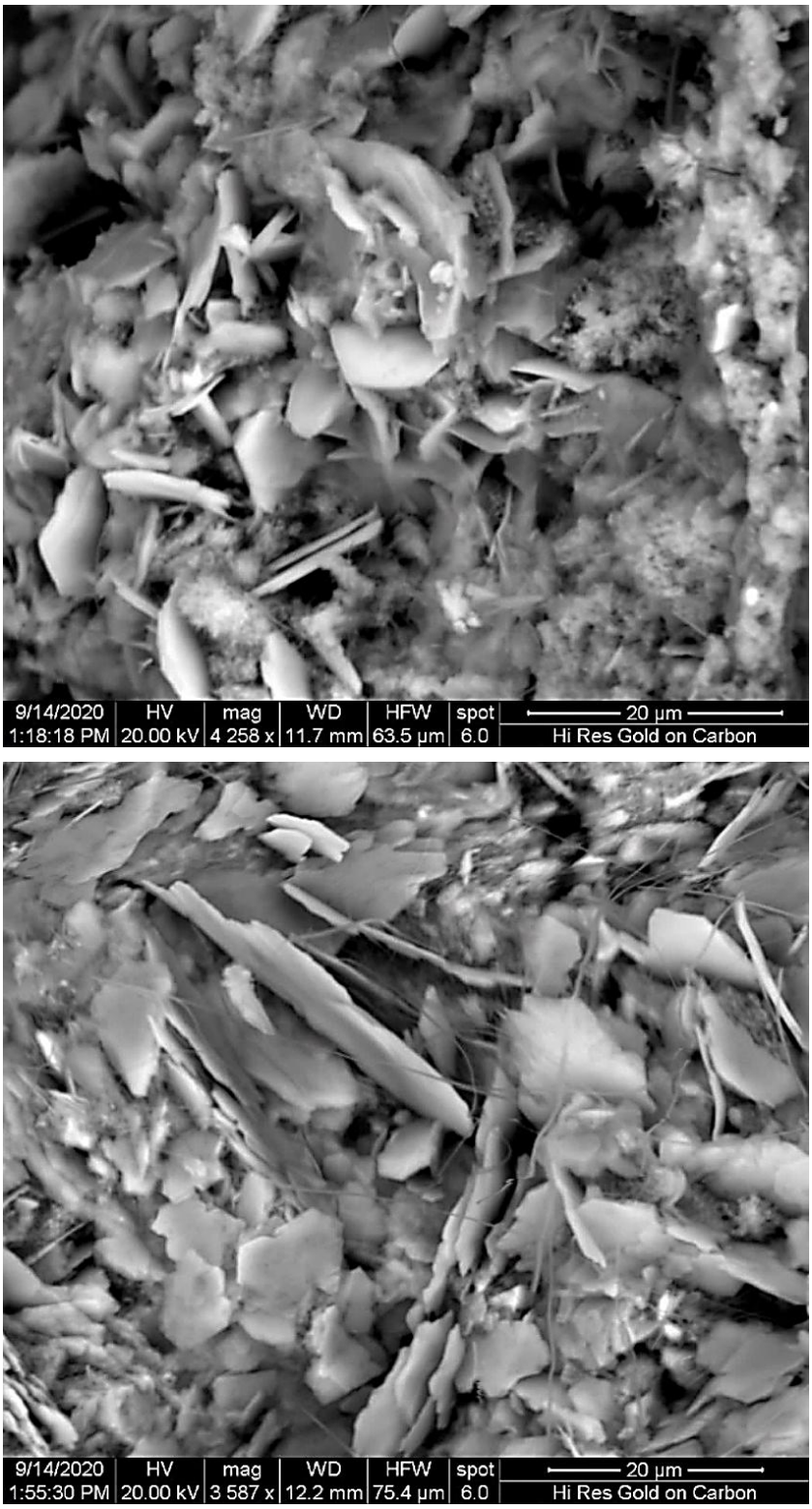

Figure 9-3. *SEM/ BSE images of calcium hydroxide crystals in the concrete at 0–60 µm (top) and 60–120 µm (bottom) from the surface of the stainless-steel object in sample 10YW-SS.*

Structural analysis of thin-section specimens showed that the cement paste has a 0–0.5 mm wide zone with slightly increased capillary porosity at the metal/concrete interface as well as some occasional small pores or blisters, Figure 9-4 and 9-5.

In addition, there is a small number of thin microcracks in a zone extending up to 3 mm from the metal surface, Figure 9-5. The origin of the microcracks is a bit uncertain with volume changes in connection with precipitation of reaction products or drying shrinkage of the concrete as the most probable mechanisms. However, some cracks may also have been formed during preparation of the thin-section specimen.

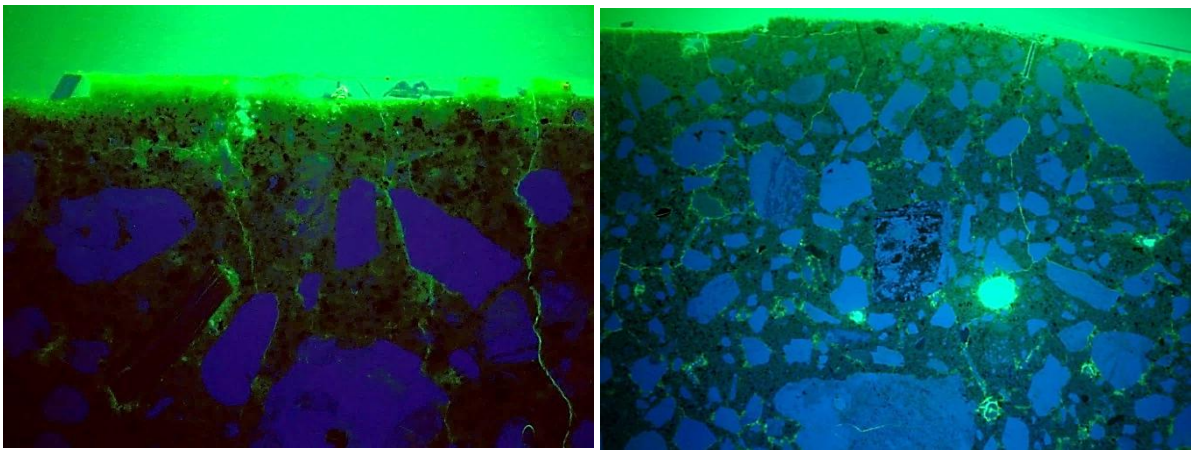

Figure 9-4. *Photographs of thin-section specimens of samples 5YW-SS (left) and 10YW-SS (right) in ultraviolet light. The images show the metal/concrete interface in the top of the image and covers an area with a width of 1.7 mm (Kalinowski 2015) and 6.7 mm (Kalinowski 2020).*

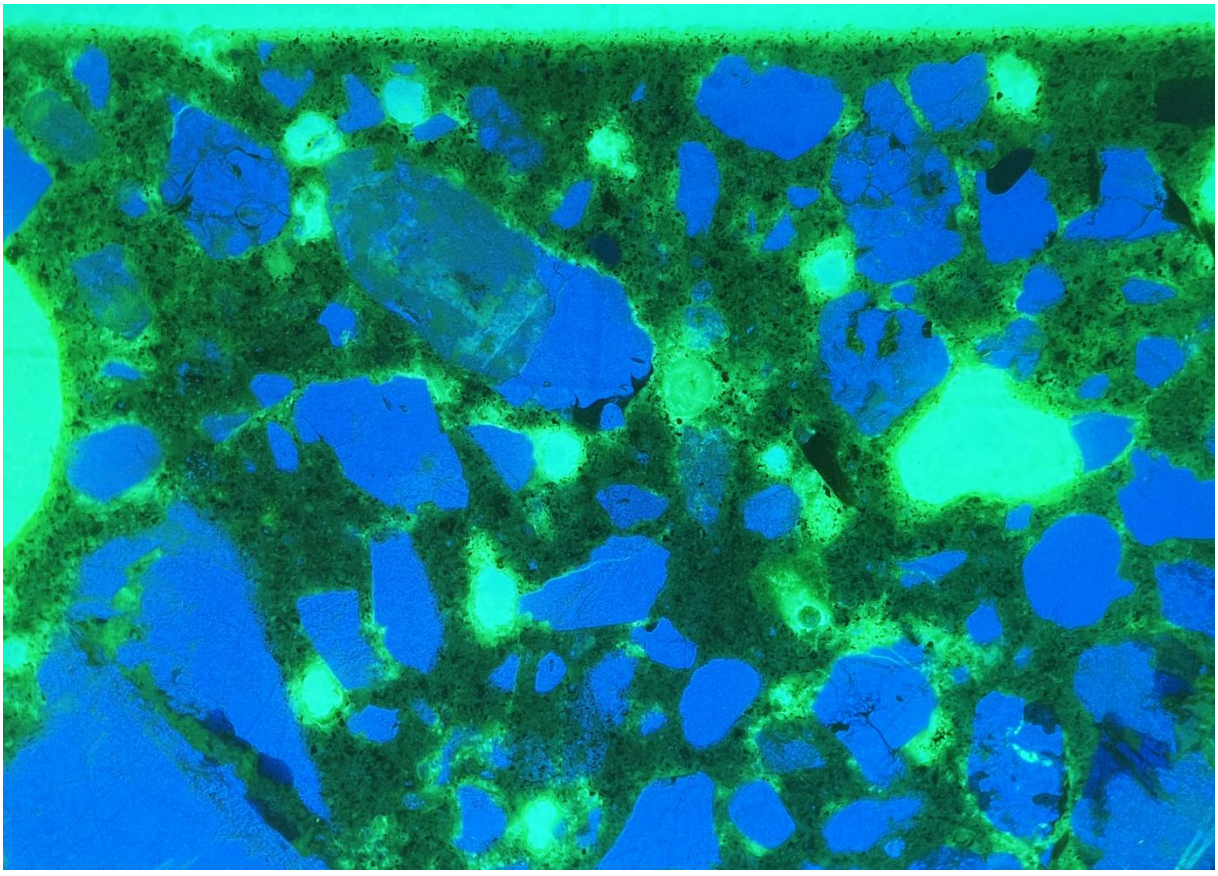

Figure 9-5. *Photograph of a thin-section specimen of sample 15YD-SS in ultraviolet light. The image shows the metal/concrete interface in the top of the image and covers an area with a width of 3.5 mm (Kalinowski 2026).*

9.4 Iron concentration profile in the cement paste

SEM/EDS analyses of the concrete close to the metal/concrete interface showed only minutely increased levels of iron (reported as Fe_2O_3) in the studied samples, Figure 9-6. However, already very close to the metal/concrete interface the average Fe_2O_3 levels were basically the same as the background level, estimated to 4.0 ± 0.3 wt. % indicating a very low corrosion rate.

These findings agree with those presented in Section 9.2.2 where corrosion products were not observed on the surface of the concrete imprint.

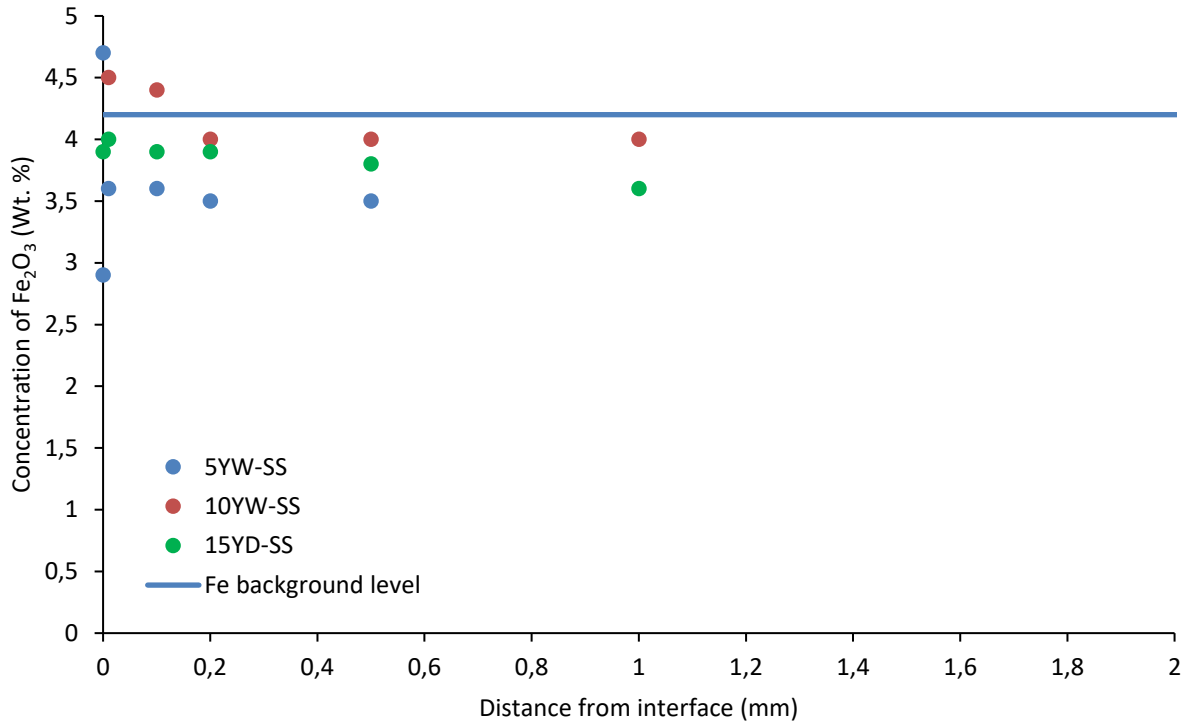

Figure 9-6. *Iron (as Fe_2O_3) concentration profiles in the concrete adjacent to the stainless-steel objects from samples 5YW-SS, 10YW- SS and 15YD- SS. Average data from the EDS-analyses also including additional elements are presented in Appendix 1.*

9.5 Summary of the observations

In this chapter, the results from long-term stainless-steel corrosion studies carried out over a period of up to 15 years at the Äspö hard rock laboratory have been presented.

The following observations have been made:

- No signs of corrosion of the stainless-steel objects were observed for any of the samples regardless of storage time and conditions.
- The appearance of the stainless-steel objects after completion of the experiments was the same as when the concrete cylinders were prepared.
- The iron concentration in the cement paste close to the metal/concrete interface was practically the same as the background level in the cement paste or lower.
- Only a slight increase of the porosity of the cement paste at the metal/concrete interface was observed. This differs significantly from the observations made for the aluminium and zinc samples where large pores filled with reaction products were found in this region but corresponds well with the appearance of the cement paste adjacent to the carbon-steel object. This type of small pores is commonly observed close to the concrete aggregates and cannot unequivocally be attributed to reactions between the cement paste and the carbon-steel objects.

10 Summary and conclusions

This report constitutes the final report from the long-term studies of metal corrosion carried out within the framework of the project *Concrete and Clay* during the years 2010 to 2025 in the Äspö Laboratory's underground facility. The report summarises the results from studies of corrosion of metal objects of aluminium, zinc, carbon steel and stainless steel which have been embedded in concrete and stored under repository-like conditions for up to 15 years.

In this chapter the results are shortly summarised, and conclusions presented. For further details, please refer to the previous chapters.

10.1 Long-term studies of zinc corrosion

Zinc reacts vigorously with the alkaline porewater of fresh concrete and the evolution of hydrogen gas during this process causes the formation of a porosus zone adjacent to the metal/concrete interface.

As a result of the corrosion process, these pores are filled with corrosion products, and a low permeability layer is formed. This layer restricts further transport of chemical species between the metal surface and the surrounding concrete which reduces the zinc corrosion rate significantly.

From the findings presented in this study it can be concluded that conditioning of zinc-containing waste in a cement-based matrix will generate significant amounts of hydrogen gas during the conditioning process. However, the protective layer of corrosion products formed during this process and during the operational period of the repository will restrict zinc corrosion post-closure.

The implication of this is that the rate of formation of hydrogen gas due to zinc corrosion during saturation of the repository post-closure will be much lower than previously assumed. This means that also the risk for fracturing of the engineered barriers due to high gas pressures inside the waste compartment and gas-driven transport of radioactive species will decrease compared to previous assessments.

The findings in this study are in accordance with those made by Herting and Odnevall (2021) who studied zinc corrosion under laboratory conditions representative for a repository for nuclear waste over a period of two years. In their study, a rapidly decreasing zinc corrosion rate was observed already during the first couple of months after experiment start.

10.2 Long-term studies of aluminium corrosion

Aluminium reacts vigorously with the alkaline porewater of fresh concrete and the evolution of hydrogen gas during this process causes the formation of a porosus zone adjacent to the metal/concrete interface.

As a result of the corrosion process, these pores are filled with corrosion products, and a low permeability layer is formed. This layer restricts further transport of chemical species between the metal surface and the surrounding concrete which reduces the aluminium corrosion rate significantly.

From the findings presented in this study it can be concluded that conditioning of aluminium-containing waste in a cement-based matrix will generate significant amounts of hydrogen gas during the conditioning process. However, the protective layer of corrosion products formed during this process and during the operational period of the repository will restrict aluminium corrosion post-closure.

The implication of this is that the rate of formation of hydrogen gas due to aluminium corrosion during saturation of the repository post-closure will be much lower than previously assumed. This means that also the risk for fracturing of the engineered barriers due to high gas pressures inside the waste compartment and gas-driven transport of radioactive species will decrease compared to previous assessments.

These findings are in accordance with those made by Herting and Odnevall (2021) who studied aluminium corrosion under laboratory conditions representative for a repository for nuclear waste over a period of two years. They found qualitatively similar behaviour over time of Al as that of Zn, although higher absolute corrosion rates for Al.

10.3 Long-term studies of carbon-steel corrosion

In this study, corrosion of the carbon-steel objects was not observed, and this study thus provides additional support for the assumptions made in (SKB 2023d) concerning the low corrosion rate of carbon steel.

10.4 Long-term studies of stainless-steel corrosion

In this study, corrosion of the stainless-steel objects was not observed.

References

SKB´s (Svensk Kärnbränslehantering AB) publications can be found at www.skb.com/publications. SKBdoc documents will be submitted upon request to document@skb.se.

Gaucher E, Tournassat C, Nowak C, 2005. Modelling the geochemical evolution of the multi-barrier system of the silo of the SFR repository. SKB R-05-80, Svensk Kärnbränslehantering AB.

Herting G, Odnevall I, 2021. Corrosion of aluminium and zinc in concrete at simulated conditions of the repository of low active waste in Sweden. Corrosion and Materials Degradation 2, 150–162.

Höglund L-O, 2014. The impact of concrete degradation on the BMA barrier functions. SKB R-13-40, Svensk Kärnbränslehantering AB.

Kalinowski M, 2015. Betongcylinder I-1B med ingjutna metallprover. Research Institute of Sweden AB, RISE. Report from assignment 5P00289. SKBdoc 1495415 version 1.0, Svensk Kärnbränslehantering AB (In Swedish)

Kalinowski M, 2020. Betongcylindrar med ingjutna metallprover. Research Institute of Sweden AB, RISE. Report from assignment 2P05245. SKBdoc 1933618 version 1.0, Svensk Kärnbränslehantering AB (In Swedish)

Kalinowski M, 2026. Betongcylindrar med ingjutna metallprover. Research Institute of Sweden AB, RISE. Report from assignment P127334. SKBdoc 2114938 version 1.0, Svensk Kärnbränslehantering AB (In Swedish)

Mårtensson P, 2015. Äspö Hard Rock Laboratory – Concrete and Clay – Installation report. SKB P-15-01, Svensk Kärnbränslehantering AB.

Mårtensson P, 2024. Cementitious materials and components in SFR, Synthesis report. SKB TR-23-18, Svensk Kärnbränslehantering AB.

Mårtensson P, Kalinowski M, 2019. Äspö Hard Rock Laboratory - Concrete and Clay - Retrieval and analysis of experimental package #20. SKB P-19-18, Svensk Kärnbränslehantering AB.

SKB, 2008. Safety analysis SFR 1. Long term safety. SKB R-08-130, Svensk Kärnbränslehantering AB.

SKB 2019. Post-closure safety for a proposed repository concept for SFL. Main report for the safety evaluation SE-SFL. SKB TR-19-01, Svensk Kärnbränslehantering AB.

SKB 2023a. Post-closure safety for SFR, the final repository for short-lived radioactive waste at Forsmark, Main report, PSAR version. SKB TR-23-01, Svensk Kärnbränslehantering AB.

SKB 2023b. Post-closure safety for SFR, the final repository for short-lived radioactive waste at Forsmark, Engineered barrier process report, PSAR version. SKB TR-23-04, Svensk Kärnbränslehantering AB.

SKB 2023c. Post-closure safety for SFR, the final repository for short-lived radioactive waste at Forsmark, Waste form and packaging process report, PSAR version. SKB TR-23-03, Svensk Kärnbränslehantering AB.

SKB 2023d. Post-closure safety for SFR, the final repository for short-lived radioactive waste at Forsmark, Data report, PSAR version, SKB TR-23-10, Svensk Kärnbränslehantering AB.

Szabó Z, Dvinskikh S, Emmer Å, Svenberg L, Wold S, Mårtensson P, 2020. Äspö Hard Rock Laboratory - Concrete and Clay - Degradation of organics materials in cementitious environments. SKB TR-20-02, Svensk Kärnbränslehantering AB.

Appendix 1

This appendix presents average values for the chemical composition of cement paste at different distances from the metal surface for the four types of metals and alloys covered in this report as a function of the duration of the experiment. The tables show average values of several analyses performed at different parts of the sample. The original full data-sets are presented in the appendices in Kalinowski (2015, 2020 and 2026) respectively. The first row of the table shows the distance from the metal surface whereas the last (distance 100 mm) is assumed to correspond to the original composition of the cement paste. This value is presented as the background concentration in the diagrams in the main part of this report showing the concentration profiles of the metals in the cement paste of the different samples.

Zinc

Table A1-1 to A1-3 present average values for the composition of the cement paste adjacent to the zinc objects. Results from individual analyses are presented in the appendices in Kalinowski (2015, 2020 and 2026) respectively.

Table A1-1. Chemical composition of the cement paste at different distances from the metal surface for sample 5YW-Zn. (Kalinowski 2015)

Distance (mm)	0	0.01	0.1	0.2	0.3	0.5	0.6	100
Oxide type	Oxide concentration (weight%)							
Na_2O	4.5	0.5	0.5	0.4	0.6	0.8	1.0	0.6
MgO	1.3	1.0	0.9	1.0	1.0	1.2	1.2	1.3
Al_2O_3	5.0	3.9	4.3	4.1	4.4	4.0	3.7	4.1
SiO_2	19.7	19.0	20.2	20.1	21.5	22.4	23.0	21.4
SO_3	3.7	2.6	2.7	2.7	3.4	3.0	2.6	2.4
K_2O	1.5	0.9	1.0	1.1	1.1	1.0	1.1	1.3
CaO	51.2	66.3	65.2	65.3	64.0	63.6	63.6	65.1
Fe_2O_3	3.6	4.7	4.5	4.7	3.8	3.9	3.8	4.0
ZnO	9.5	1.1	0.7	0.5	0.2	0.0	0.0	0.0
Total	100	100	100	100	100	100	100	100

Table A1-2. Chemical composition of the cement paste at different distances from the metal surface for sample 10YW-Zn. (Kalinowski 2020)

Distance (mm)	0–0.06	0.06–0.12	0.12–0.18	0.18–0.24	0.3	0.4	0.5	1
Oxide type	Oxide concentration (weight%)							
Na_2O	0.4	0.2	0.2	0.4	0.2	0.2	0.3	0.3
MgO	0.9	1.0	1.4	1.0	1.3	1.4	1.4	1.1
Al_2O_3	3.9	4.0	5.7	4.3	4.8	4.4	4.4	3.6
SiO_2	19.7	22.1	28.0	20.5	24.9	23.9	24.1	22.2
SO_3	2.4	2.0	2.5	2.6	2.9	2.9	2.9	2.5
K_2O	1.1	0.3	0.8	0.8	0.4	0.2	0.5	0.5
CaO	66.5	65.0	56.7	65.3	61.3	62.5	62.1	65.0
TiO_2	0.2	0.2	0.2	0.2	0.2	0.2	0.2	0.2
Fe_2O_3	4.7	4.8	4.3	4.6	4.0	4.2	4.0	4.5
ZnO	0.3	0.2	0.2	0.1	0.0	0.0	0.0	0.0
Total	100	100	100	100	100	100	100	100

Table A1-3. Chemical composition of the cement paste at different distances from the metal surface for sample 15YD-Zn. (Kalinowski 2026)

Distance (mm)	0	0.01	0.06	0.08	0.09	0.11	0.16	0.21
Oxide type	Oxide concentration (weight%)							
Na_2O	1.6	1.3	1.1	1.6	1.4	1.0	2.2	1.8
MgO	0.8	0.8	1.1	1.1	0.6	0.9	1.0	0.8
Al_2O_3	3.6	4.2	3.7	4.4	3.5	4.2	4.3	3.6
SiO_2	20.2	20.1	18.3	21.6	21.1	20.4	22.5	21.3
SO_3	2.2	2.6	3.4	3.0	1.3	3.1	2.2	1.5
K_2O	2.5	3.0	1.7	1.8	3.8	1.9	2.4	3.5
CaO	64.4	62.8	65.9	62.1	64.1	64.2	61.8	63.4
TiO_2	0.3	0.3	0.3	0.3	0.2	0.3	0.2	0.2
Fe_2O_3	3.7	4.2	4.1	3.9	3.3	3.9	3.3	3.5
ZnO	0.7	0.7	0.4	0.3	0.5	0.2	0.1	0.3
Total	100	100	100	100	100	100	100	100

Table A1-3 (continued). Chemical composition of the cement paste at different distances from the metal surface for sample 15YD-Zn - continued. (Kalinowski 2026)

Distance (mm)	0.26	0.31	0.41	0.49	0.51	0.56	0.61	0.71
Oxide type	Oxide concentration (weight%)							
Na_2O	0.4	1.8	1.8	2.0	1.5	1.6	1.7	1.7
MgO	1.3	0.5	0.8	0.9	0.6	0.6	0.7	0.8
Al_2O_3	4.9	3.2	3.9	4.1	2.7	2.5	3.6	3.8
SiO_2	20.8	19.1	20.4	18.1	18.5	19.7	19.6	16.8
SO_3	4.1	1.1	1.0	1.5	0.9	1.1	0.7	0.6
K_2O	0.5	4.2	4.3	3.4	3.9	4.5	4.3	4.3
CaO	63.4	65.7	64.0	65.7	68.4	66.6	65.5	68.6
TiO_2	0.2	0.3	0.3	0.3	0.2	0.2	0.2	0.2
Fe_2O_3	4.2	3.8	3.2	4.1	3.2	3.3	3.6	3.1
ZnO	0.2	0.2	0.2	0.0	0.0	0.0	0.0	0.0
Total	100	100	100	100	100	100	100	100

Aluminium

Table A1-4 and A1-5 present average values for the composition of the cement paste adjacent to the aluminium objects. Results from individual analyses are presented in the Appendices in Kalinowski (2015 and 2020) respectively.

Table A1-4. Chemical composition of the cement paste at different distances from the metal surface for sample 5YW-Al. (Kalinowski 2015)

Distance (mm)	0	0.05	0.16	0.25	0.35	0.45	0.55	0.65	0.75
Oxide type	Oxide concentration (weight%)								
Na_2O	1.4	0.5	0.6	0.4	0.5	0.6	0.6	0.4	0.4
MgO	1.3	0.8	0.7	0.7	0.7	0.7	0.7	0.6	1.1
Al_2O_3	88.7	72.4	53.6	24.1	21.8	20.7	22.1	17.9	15.3
SiO_2	5.0	6.1	9.8	15.3	14.8	16.5	16.5	15.4	20.0
SO_3	0.1	0.6	1.0	1.7	1.9	2.3	2.1	3.2	2.4
K_2O	2.7	1.8	1.7	1.6	1.9	1.7	1.8	1.7	1.4
CaO	0.3	16.1	30.1	52.1	54.5	53.5	52.2	57.1	54.4
Fe_2O_3	0.6	1.8	2.5	4.1	3.9	3.9	4.0	3.6	5.0
Total	100	100	100	100	100	100	100	100	100

Table A1-4 (Continued). Chemical composition of the cement paste at different distances from the metal surface for sample 5YW-Al - Continued. (Kalinowski 2015)

Distance (mm)	0.85	0.95	1.05	1.2	1.3	1.4	1.5	100
Oxide type	Oxide concentration (weight%)							
Na_2O	0.6	0.5	0.8	0.8	0.3	0.3	0.2	1.1
MgO	1.0	0.8	1.2	1.1	0.9	1.0	1.0	1.4
Al_2O_3	9.8	5.8	8.1	7.7	5.2	4.6	3.7	4.5
SiO_2	20.8	19.1	19.9	22.0	20.4	22.4	20.2	24.6
SO_3	2.8	3.0	2.8	2.7	3.1	3.3	2.5	2.2
K_2O	1.6	1.2	0.8	0.7	0.8	0.5	0.4	1.4
CaO	59.6	65.1	62.3	61.3	65.0	63.9	67.7	60.7
Fe_2O_3	3.7	4.3	4.1	3.7	4.2	4.0	4.3	4.2
Total	100	100	100	100	100	100	100	100

Table A1-5. Chemical composition of the cement paste at different distances from the metal surface for sample 10YW-Al. (Kalinowski 2020)

Distance (mm)	0-0.05	0.05	0.5	1	2	3	5
Oxide type	**Oxide concentration (weight%)**						
Na_2O	0.7	0.7	0.4	0.2	0.3	0.3	0.2
MgO	0.8	0.8	0.8	1.0	1.1	1.2	1.1
Al_2O_3	39.7	36.9	19.0	6.0	4.9	4.3	3.8
SiO_2	13.4	14.3	17.4	21.9	24.0	23.9	22.1
SO_3	1.4	1.8	4.2	2.9	2.7	2.7	2.4
K_2O	3.3	3.2	1.2	0.5	0.5	0.6	0.3
CaO	37.3	38.9	53.4	63.1	62.6	63.1	65.8
TiO_2	0.2	0.2	0.2	0.2	0.3	0.2	0.2
Fe_2O_3	3.2	3.2	3.4	4.2	3.7	3.8	4.2
Total	100	100	100	100	100	100	100

Carbon steel

Table A1-6 to A1-8 present average values for the composition of the cement paste adjacent to the carbon-steel objects. Results from individual analyses are presented in the appendices in Kalinowski (2015, 2020 and 2026) respectively.

Table A1-6. Chemical composition of the cement paste at different distances from the metal surface for sample 5YW-CS. (Kalinowski 2015)

Distance (mm)	0	0.01	0.1	0.2	0.3	0.5	100
Oxide type	**Oxide concentration (weight%)**						
Na_2O	0.7	1.1	1.7	1.6	2.2	2.1	1.5
MgO	0.9	1.2	0.9	0.9	1.0	1.1	1.2
Al_2O_3	3.7	3.8	3.5	3.3	3.6	3.6	4.1
SiO_2	18.2	22.9	22.4	22.0	23.1	23.0	24.0
SO_3	1.1	2.2	2.3	2.4	2.4	2.2	2.4
K_2O	3.0	1.3	1.5	1.9	2.0	1.7	1.5
CaO	66.9	63.5	64.0	64.3	61.9	62.4	61.0
Fe_2O_3	5.4	4.0	3.6	3.6	3.8	3.8	4.3
Total	100	100	100	100	100	100	100

Table A1-7. Chemical composition of the cement paste at different distances from the metal surface for sample 10YW-CS. (Kalinowski 2020)

Distance (mm)	0-0.03	0.05	0.5	1	12	13	14	15	16	100
Oxide type	**Oxide concentration (weight%)**									
Na_2O	0.4	0.6	0.5	0.5	1.1	0.3	1.5	0.9	0.6	0.3
MgO	1.5	1.4	1.4	1.8	1.3	1.3	1.2	1.1	1.1	1.3
Al_2O_3	4.9	4.7	4.6	4.8	4.5	3.9	4.2	4.0	3.5	4.4
SiO_2	24.0	25.1	24.2	24.7	24.4	23.4	23.5	23.2	22.6	24.4
SO_3	2.8	2.9	2.7	2.6	1.4	2.3	1.2	2.0	1.5	2.5
K_2O	0.5	0.9	0.8	0.9	1.4	0.5	2.0	1.3	1.6	0.5
CaO	61.4	60.0	61.3	59.9	61.4	63.9	62.0	63.4	64.6	62.4
TiO_2	0.3	0.2	0.2	0.3	0.3	0.2	0.2	0.2	0.3	0.2
Fe_2O_3	4.1	4.2	4.2	4.5	4.2	4.3	4.0	3.9	4.2	4.0
Total	100	100	100	100	100	100	100	100	100	100

Table A1-8. Chemical composition of the cement paste at different distances from the metal surface for sample 15YD-CS. (Kalinowski 2026)

Distance (mm)	0	0.01	0.06	0.11	0.21	0.31	0.41	0.51	1.01
Oxide type	Oxide concentration (weight%)								
Na_2O	2.2	2.3	1.9	1.5	2.1	2.5	2.2	2.1	3.3
MgO	0.9	1.4	1.5	1.2	1.2	1.2	1.1	1.2	1.1
Al_2O_3	3.7	4.5	4.7	4.1	4.3	4.2	4.0	4.1	4.5
SiO_2	19.1	23.8	25.2	25.8	25.5	24.8	24.6	24.6	23.9
SO_3	23	4.5	4.6	4.4	4.3	4.1	3.6	3.8	3.6
K_2O	4.2	2.3	1.8	1.2	1.4	1.6	1.9	1.6	2.3
CaO	62.2	57.4	56.3	58.3	58.0	57.9	58.9	58.9	7.5
TiO_2	0.3	0.4	0.4	0.3	0.2	0.4	0.3	0.3	0.3
Fe_2O_3	5.1	3.5	3.5	3.2	3.2	3.3	3.5	3.4	3.5
Total	100	100	100	100	100	100	100	100	100

Stainless steel

Table A1-9 to A1-11 present average values for the composition of the cement paste adjacent to the stainless-steel objects. Results from individual analyses are presented in the appendices in Kalinowski (2015, 2020 and 2026) respectively.

Table A1-9. Chemical composition of the cement paste at different distances from the metal surface for sample 5YW-SS. (Kalinowski 2015)

Distance (mm)	0	0	0.01	0.1	0.2	0.5	100
Oxide type	**Oxide concentration (weight%)**						
Na_2O	0.7	1.1	0.9	0.6	1.2	1.3	0.8
MgO	1.6	3.4	2.0	1.3	1.4	1.2	1.7
Al_2O_3	9.9	4.1	4.8	4.1	4.4	3.9	4.7
SiO_2	37.5	17.8	26.1	24.8	24.9	24.5	24.9
SO_3	2.4	4.3	2.8	2.7	2.8	2.9	3.6
K_2O	1.4	2.6	0.8	0.6	0.8	1.0	1.1
CaO	41.8	63.8	58.9	62.3	60.9	61.6	59.0
Fe_2O_3	4.7	2.9	3.6	3.6	3.5	3.5	4.2
Total	100	100	100	100	100	100	100

Table A1-10. Chemical composition of the cement paste at different distances from the metal surface for sample 10YW-SS. (Kalinowski 2020)

Distance (mm)	0-0.06	0.06-0.12	0.2	0.5	1	3	10
Oxide type	**Oxide concentration (weight%)**						
Na_2O	0.5	0.7	0.8	0.8	1.0	0.4	0.9
MgO	1.0	0.9	1.3	1.1	1.1	1.1	1.4
Al_2O_3	4.5	4.1	4.5	4.1	4.1	3.9	4.7
SiO_2	17.7	18.3	21.3	20.9	21.7	22.3	24.1
SO_3	2.4	2.6	2.4	2.1	2.3	2.2	2.1
K_2O	1.1	1.3	1.1	1.1	1.3	0.7	0.9
CaO	68.2	67.4	64.4	65.6	64.2	65.1	62.1
TiO_2	0.2	0.2	0.3	0.2	0.2	0.2	0.2
Fe_2O_3	4.5	4.4	4.0	4.0	4.0	4.1	3.7
Total	100	100	100	100	100	100	100

Table A1-11. Chemical composition of the cement paste at different distances from the metal surface for sample 15YD-SS. (Kalinowski 2026)

Distance (mm)	0	0.01	0.06	0.11	0.13	0.21	0.31	0.41	0.51	1.01
Oxide type	Oxide concentration (weight%)									
Na_2O	2.5	2.2	1.0	1.0	0.7	1.2	1.0	0.5	0.6	0.7
MgO	0.7	1.1	0.7	1.2	0.9	0.9	0.8	0.7	0.8	0.9
Al_2O_3	3.9	4.0	3.2	3.6	2.9	3.7	3.4	3.1	3.3	3.5
SiO_2	20.8	22.1	20.4	21.6	19.0	22.2	21.4	18.8	22.2	22.4
SO_3	2.8	3.2	3.7	3.7	3.4	3.6	3.6	3.7	4.0	4.3
K_2O	5.8	3.4	1.4	1.5	1.8	1.7	1.4	1.0	0.9	1.0
CaO	59.2	59.8	65.3	63.3	67.5	62.6	64.1	67.9	64.0	63.2
TiO_2	0.3	0.3	0.3	0.3	0.2	0.3	0.3	0.2	0.3	0.3
Cr_2O_3	0.1	0.0	0.0	0.0	0.0	0.0	0.0	0.0	0.0	0.0
Fe_2O_3	3.8	4.0	3.9	3.9	3.7	3.9	3.9	4.1	3.8	3.6
Total	100	100	100	100	100	100	100	100	100	100